Journal of Human Evolution 62 (2012) 533–547

Contents lists available at SciVerse ScienceDirect

Journal of Human Evolution

journal homepage: www.elsevier.com/locate/jhevol

New ages for Middle and Later Stone Age deposits at Mumba rockshelter, Tanzania: Optically stimulated luminescence dating of quartz and feldspar grains

Luke A. Gliganic [a], Zenobia Jacobs [a,*], Richard G. Roberts [a], Manuel Domínguez-Rodrigo [b], Audax Z.P. Mabulla [c]

[a] Centre for Archaeological Science, School of Earth and Environmental Sciences, University of Wollongong, Wollongong, NSW 2522, Australia
[b] Departamento de Prehistoria, Universidad Complutense de Madrid, 28040 Madrid, Spain
[c] Archaeology Unit, University of Dar es Salaam, PO Box 35050, Dar es Salaam, Tanzania

ARTICLE INFO

Article history:
Received 13 September 2011
Accepted 13 February 2012
Available online 17 March 2012

Keywords:
East Africa
Chronology
Single grains
Dose distributions
Past environments

ABSTRACT

The archaeological deposits at Mumba rockshelter, northern Tanzania, have been excavated for more than 70 years, starting with Margit and Ludwig Köhl-Larsen in the 1930s. The assemblages of Middle Stone Age (MSA) and Later Stone Age (LSA) artefacts collected from this site constitute the type sequences for these cultural phases in East Africa. Despite its archaeological importance, however, the chronology of the site is poorly constrained, despite the application since the 1980s of several dating methods (radiocarbon, uranium-series and amino acid racemisation) to a variety of materials recovered from the deposits. Here, we review these previous chronologies for Mumba and report new ages obtained from optically stimulated luminescence (OSL) and infrared stimulated luminescence (IRSL) measurements on single grains of quartz and multi-grain aliquots of potassium (K) feldspar from the MSA and LSA deposits. Measurements of single grains of quartz allowed the rejection of unrepresentative grains and the application of appropriate statistical models to obtain the most reliable age estimates, while measurements of K-feldspars allowed the chronology to be extended to older deposits. The seven quartz ages and four K-feldspar ages provide improved temporal constraints on the archaeological sequence at Mumba. The deposits associated with the latest Kisele Industry (Bed VI-A) and the earliest Mumba Industry (Bed V) are dated to 63.4 ± 5.7 and 56.9 ± 4.8 ka (thousands of years ago), respectively, thus constraining the time of transition between these two archaeological phases to ~60 ka. An age of 49.1 ± 4.3 ka has been obtained for the latest deposits associated with the Mumba Industry, which show no evidence for post-depositional mixing and contain ostrich eggshell (OES) beads and abundant microlithics. The Nasera Industry deposits (Bed III) contain large quantities of OES beads and date to 36.8 ± 3.4 ka. We compare the luminescence ages with the previous chronologies for Mumba, and briefly discuss how the revised chronology fits in the context of existing archaeological records and palaeoclimatic reconstructions for East Africa.

Introduction

Mumba rockshelter contains one of the richest and most continuous Middle Stone Age (MSA) to Iron Age archaeological sequences in East Africa. Its MSA and Later Stone Age (LSA) assemblages, in particular, have become the type sequences for these cultural phases in East Africa. The best known and most notable feature is the presence of geometric microlithic stone artefacts and ostrich eggshell (OES) beads found throughout a large portion of the sequence. Microlithic technologies and the manufacture of personal ornaments play a central role in deliberations about the origins of modern human behaviour, the dispersals of modern humans within and out of Africa, and their responses to factors such as climate change (e.g., Ambrose, 1998, 2002; Wurz, 1999; McBrearty and Brooks, 2000; Mellars, 2006; McCall, 2007; Clarkson et al., 2009; Jacobs and Roberts, 2009; Petraglia et al., 2009). The abundant occurrence of microlithics and personal ornaments in the archaeological record is often used to differentiate between the LSA and MSA in Africa (Ambrose, 1998, 2002). Although they are the hallmark of the LSA, it is well known that they also occur in some MSA contexts, such as the Howieson's Poort in southern Africa, thereby obscuring the clear distinction between

* Corresponding author.
E-mail address: zenobia@uow.edu.au (Z. Jacobs).

0047-2484/$ – see front matter © 2012 Elsevier Ltd. All rights reserved.
doi:10.1016/j.jhevol.2012.02.004

the MSA and the LSA, and the timing of the transition between them.

This ambiguity applies also to Mumba, where the 'Mumba Industry' in Bed V was defined by Mehlman (1989) as a 'transitional' industry between the MSA and LSA, based on the co-occurrence of LSA-like geometric microlithics and knives, OES beads, and MSA-like stone points. The transitional nature of the assemblage, the presence of microlithic tools, and their reduction in size and increased abundance in the younger deposits at the site have been interpreted by some researchers as supporting the gradual emergence of modern human behaviour within the African MSA (e.g., McBrearty and Brooks, 2000; Henshilwood and Marean, 2003; Mellars, 2006). On the basis of amino acid racemisation (AAR) ages of 45–65 thousands of years ago (ka) for ostrich eggshell from Mumba, McBrearty and Brooks (2000) suggested that the rockshelter contains the earliest evidence for geometric microlithic tools in East Africa. These tools, together with the occurrence of OES beads, portable art (a cross-hatched OES fragment) and ochre (stones with red colour traces and ochre fragments) in Bed V and lower Bed III, were taken by McBrearty and Brooks (2000) as indicators of complex human behaviour, supporting their model for the gradual development of modern human behaviour from the earliest MSA. Deacon and Deacon (1999) noted the similarity between the Howieson's Poort (65–59 ka) in southern Africa and the backed artefacts from Mumba, and linked this to the distribution of 'click' language speakers in these two regions to infer the long-distance dispersal and exchange of ideas. Mellars (2006) proposed that the earliest microlithic toolmakers in Africa may have been among the first populations that spread to other parts of the world, including South Asia. As evidence, he drew comparisons between the microlithic tools in southern and East Africa with those in India and Sri Lanka. Others have used the same assemblages to argue for the independent development of microlithic technology in South Asia about 35 ka, in response to increasing population size and deteriorating environmental conditions (e.g., Clarkson et al., 2009; Petraglia et al., 2009).

Until recently, such comparisons have been based on the original assemblage for Mumba rockshelter, collected by Margit and Ludwig Köhl-Larsen in the 1930s, which is thought to be heavily biased against smaller artefacts and to favour, instead, larger cores and flakes made from exotic materials such as obsidian and chert (Mehlman, 1989). The collection of artefacts excavated subsequently by Mehlman is incomplete and mostly unstudied (Mehlman, 1989; Prendergast et al., 2007; Diez-Martín et al., 2009). In addition, the Köhl-Larsen and Mehlman excavations were dug in spit depths of 20–40 cm and 10 cm, respectively, and assumed that the deposit was formed by the accumulation of horizontal beds (Prendergast et al., 2007). Mehlman also suggested that the Mumba deposits and the associated artefacts had been mixed after burial, so that the archaeological levels cannot be clearly distinguished (Mehlman, 1989; Prendergast et al., 2007). Furthermore, the ages reported thus far for Mumba have been obtained using sample preparation and measurement procedures that are no longer considered reliable or that were applied to unsuitable materials (e.g., uranium-series dating of bone), and ages have also been published without any associated uncertainties or supporting information.

Given these archaeological and chronological shortcomings, new excavations were undertaken at Mumba rockshelter in 2005 to facilitate a complete reassessment of site formation and stratigraphy, and to obtain an unbiased artefact assemblage for typological and technological characterisation. Importantly, Prendergast et al. (2007) showed that the entire deposit had not accumulated as a series of horizontal beds. Instead, they observed significant lateral and vertical changes within each level and were able to discriminate between different geological units on the basis of their separation by thin layers of culturally sterile sediments and distinct layers of rock fall. Their observations cast doubt on the presumption of contemporaneity of artefacts collected from relatively thick and horizontal spits by the previous excavators. In addition, the supposed 'transitional' nature of the assemblage was not supported by Diez-Martín et al. (2009), who performed a systematic analysis of the technology and typology of the unbiased artefact assemblage newly excavated from levels equivalent to Bed V of Mehlman and the Köhl-Larsens. They found no evidence for technological change or for MSA attributes. Instead, their entire 'Bed V' assemblage was consistent with LSA technology, containing a large proportion of tools produced using the bipolar technique. From their typological analysis, however, they observed a change in the relative abundance and size of geometric microlithics between the lower and upper levels, but could not discount the possibility that this change was a function of the limited sample size.

In both southern and East Africa, it has become increasingly evident that defining the LSA and MSA, and the transition between them, is not straightforward. The technological and typological approaches that have customarily been used to differentiate between these periods do not yield unambiguous results. A possible means of surmounting this predicament is to compare and contrast assemblages based on their numerical ages. Resolving subtle differences in timing, however, can only be achieved if a common chronology is constructed for all assemblages at a given site. To this end, we collected sediment samples from Mumba rockshelter in 2007 for optically stimulated luminescence (OSL) dating. We used the new stratigraphic sequence of Prendergast et al. (2007) to securely tie the OSL sample locations to well-defined archaeological units from which unbiased artefact assemblages have been examined using current technological and traditional typological approaches (Diez-Martín et al., 2009). By dating the Mumba samples with the same instruments and procedures as employed at several other African sites, we can align the Mumba sequence on the same timeline as archaeological sequences in southern Africa (Jacobs et al., 2008a) and search for common patterns that might link these two regions.

The aim of this paper, therefore, is four-fold:

- To provide numerical age estimates for the Mumba microlithics and for the most recent pre-microlithic (MSA) levels in the sequence (Diez-Martín et al., 2009).
- To directly test the claims for stratigraphic integrity of the most recently excavated deposits at Mumba (Prendergast et al., 2007).
- To assess the temporal (dis)continuity of the revised archaeological and sedimentological sequences proposed by Diez-Martín et al. (2009) and Prendergast et al. (2007), respectively.
- To assess possible reasons for changes in technology at Mumba by comparing their timing with existing archaeological and palaeoclimatic records for East Africa.

Site setting, stratigraphy and archaeological context

Mumba rockshelter (3°17′47″E, 3°32′26″S) is located ~1050 m above mean sea level on the southeastern side of Lake Eyasi in northern Tanzania, ~62 km south of Olduvai Gorge (Fig. 1). The Lake Eyasi basin is situated near the southwestern terminus of the Crater Highlands volcanic area, but volcanic debris is found only in the northernmost portion of the lake and does not reach the rockshelter. The basin is of Pleistocene age and is now filled mostly with sediment. When dry, the lakebed is subject to severe aeolian deflation by strong northerly winds, but the lake level has

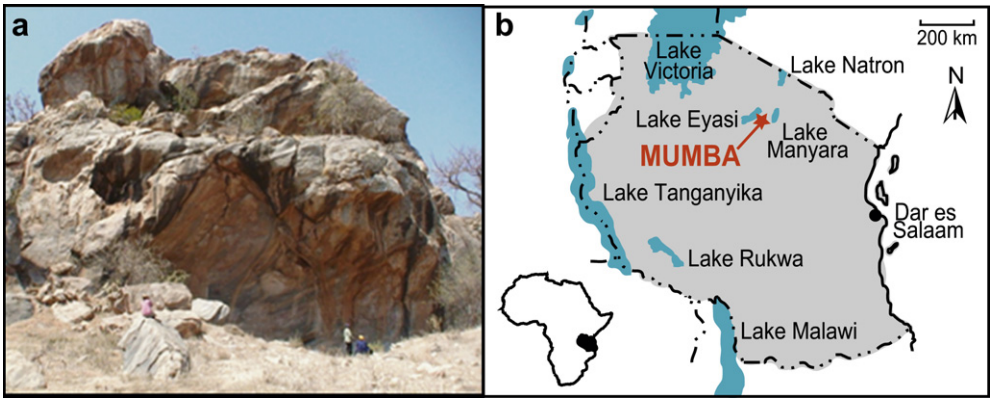

Figure 1. a. Photograph of Mumba rockshelter. The excavated deposits lie immediately behind the two people in the centre foreground. b. Map of Tanzania showing the locations of Mumba rockshelter, Lake Eyasi and other lakes in the region.

also been high enough at times to submerge Mumba rockshelter (Prendergast et al., 2007). Today, the modern lake is approximately 2–4 km from the site, depending on the lake level, which continues to fluctuate significantly. The rockshelter is located at the base of a massive outcrop of Precambrian diorite and gneiss. This block of metamorphic rock has a slight overhang that is barely noticeable, so the site is not a rockshelter that affords much protection from the elements.

Mumba was first excavated by the Köhl-Larsens, who removed most of the deposit (9 × 12.5 × 10.75 m) between 1934 and 1938 (Fig. 2c). The site was later revisited by Mehlman, who excavated a further four 'witness' sections in 1979 and 1981 to refine the stratigraphy of the site and to obtain samples for purposes of dating (Mehlman, 1989). Margit Köhl-Larsen identified six geological beds in more than 10 m depth of deposit, and named them Beds I to VI (Köhl-Larsen, 1943). Mehlman retained this nomenclature when he analysed the Köhl-Larsen lithic assemblage and defined the archaeological sequence for the site (Mehlman, 1989). In 2005, the site was re-excavated by a team led by Domínguez-Rodrigo and Mabulla. They opened up four trenches along the perimeter of the area excavated by the Köhl-Larsens, and named them Trenches 5 to 8 (Fig. 2c and d).

To reassess the overall stratigraphy and history of formation of the site, Prendergast et al. (2007) examined cleaned exposures of the original Köhl-Larsen and Mehlman excavations, in addition to section profiles of the four new trenches. They subdivided the deposit into a sequence of eight geological units, and named them Units A (at the top) to H (at the base). The units are differentiated primarily by the relative abundance of stone blocks and slabs, alternating between units composed of fine-grained aeolian sediments (silts and sands) and units containing rocks (≥10 cm) embedded in a silt-sand matrix. A number of archaeologically sterile units, each ~10 cm thick, were also identified by Prendergast et al. (2007), who give detailed descriptions of each of the new geological units and a history of research at Mumba. The silts and sands were likely derived from deflation of the exposed lakebed during drier periods, whereas the cobbles were transported by gravity from a fracture on the eastern side of the

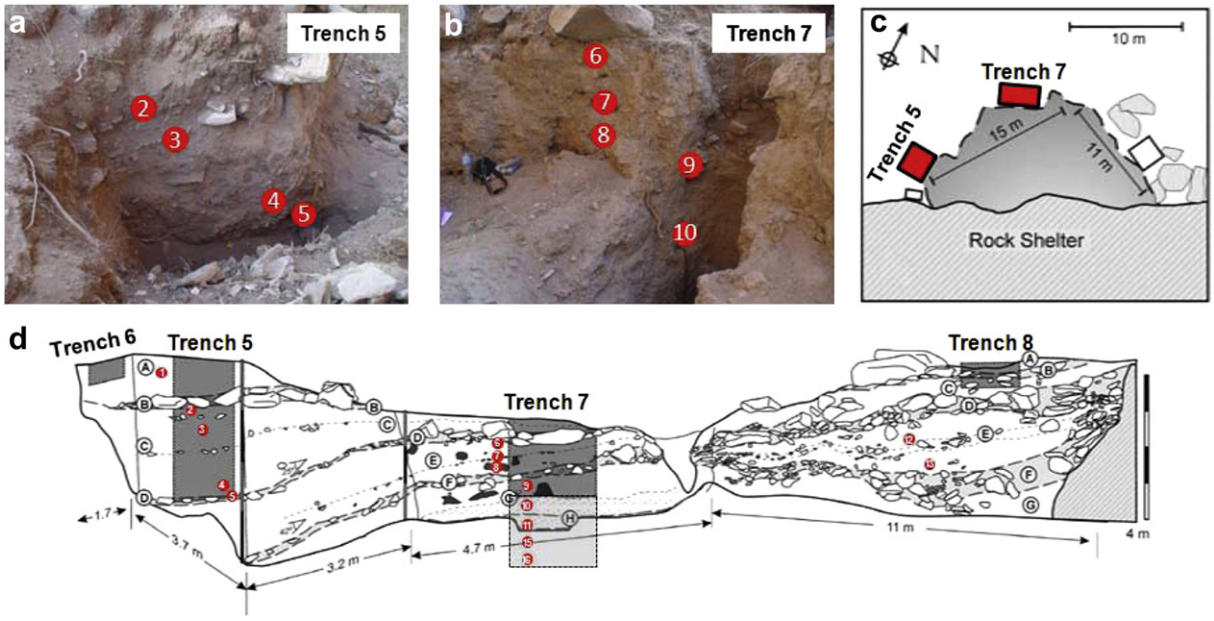

Figure 2. Photographs of the deposits in a. Trench 5 and b. Trench 7, with the approximate locations of OSL samples MR2–10 shown as red circles. c. Planview of the rockshelter, with Trenches 5 and 7 marked as red boxes. d. Stratigraphic drawing of the cleaned exposures, with the geological units of Prendergast et al. (2007) labelled A–H and the approximate positions of fifteen OSL samples shown as red circles. In a, b and d, the red circles are overlain by the OSL sample codes. (For interpretation of the references to color in this figure legend, the reader is referred to the web version of this article.)

rockshelter and as rock fall. The different units are easiest to distinguish in the east and north of the site and less conspicuous further west, where the rocks are fewer and smaller (Fig. 2d). As a result of this lateral variation, the contact between units is rarely horizontal and each unit is of variable thickness across the exposure (Prendergast et al., 2007). Fig. 3 is a schematic section showing the relation between the eight geological units of Prendergast et al. (2007) and the six geological beds of Mehlman (1989), together with the lithic industries as defined by Mehlman (1989).

Mehlman (1989) based his archaeological sequence on a typological assessment of the biased Köhl-Larsen assemblage, and his terminology for Mumba is still widely used. Diez-Martín et al. (2009) revised only the Bed V assemblage, so the general validity of Mehlman's scheme remains to be tested using the unbiased artefact assemblage collected from the 2005 excavations. We recognise, therefore, that the following summary of the archaeological sequence proposed by Mehlman (1989) may be subject to revision.

The basal deposits of the excavated sequence (Unit H, Bed VI-B) contained stone artefacts assigned to the Sanzako Industry. This industry is characterised by high frequencies of side- and notched-scrapers, bifacially modified pieces and heavy-duty tools, such as small bifaces and choppers. Levallois technology and points are rare (Mehlman, 1989; Mabulla, 2007). The base of the overlying unit (Unit G) corresponds to Bed VI-A and is associated with the Kisele Industry, which is characterised by high frequencies of disc and part-peripheral cores. Bifacial and unifacial points and scrapers are the most distinctive tool types (Mehlman, 1989). The 2005 assemblage also contained large-sized artefacts, such as Levallois cores and large scrapers, but lacked any microlithics (Diez-Martín et al., 2009).

Overlying these deposits is Mehlman's Bed V, which is equivalent to the upper part of Unit G, all of Units F and E, and the lower part of Unit D in the geological scheme of Prendergast et al. (2007). Mehlman (1989) proposed that Bed V contained a transitional industry, which he termed the Mumba Industry, with components that can be described as MSA (e.g., retouched points) and LSA (e.g., geometric microlithics and knives). By contrast, the unbiased Bed V assemblage collected from Trench 7 in 2005 did not contain any retouched points or knives (Diez-Martín et al., 2009). This discrepancy complicates a straightforward comparison with the Mehlman record, and raises the possibility that some of these elements were incorporated in the original assemblage as a result of being excavated in thick, horizontal spits (Prendergast et al., 2007). An alternative explanation is that the most recent excavations were on the periphery of those made by the Köhl-Larsens and Mehlman, so some of the differences between the artefact assemblages may reflect spatial variations across the site.

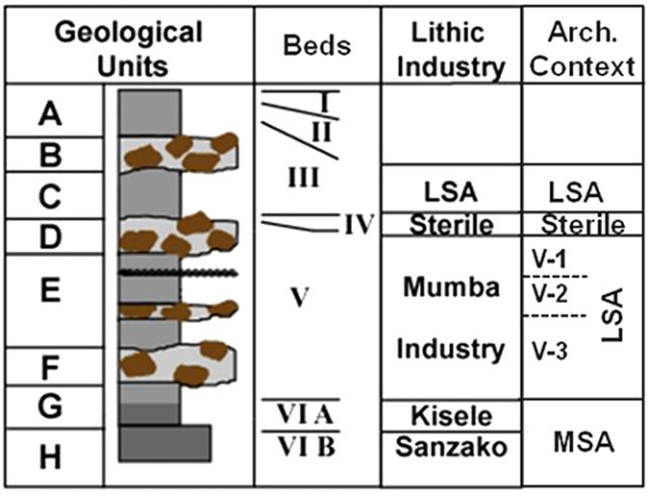

Figure 3. Schematic cross-section indicating the relation between the geological units of Prendergast et al. (2007), the beds of Mehlman (1989) and the associated lithic industries of Mehlman (1989) and Diez-Martín et al. (2009). The Mumba Industry was assigned to the MSA/LSA transition by Mehlman and to the LSA by Diez-Martín et al. (2009).

Diez-Martín et al. (2009) divided the 2005 Bed V assemblage into lower, middle and upper sections. This tripartite division mimicked that made by Mehlman (1989) during his assessment of the Bed V artefact assemblage, and reflected the observation that the artefacts in the middle section appeared to be separated from those below by a conspicuous layer of medium-sized rocks in Unit E, and from those above by a ~10 cm-thick layer of sterile sand (Fig. 3) (Prendergast et al., 2007; Diez-Martín et al., 2009). They found that the overall properties of the Bed V assemblage could be classified as LSA. They observed a distinct shift towards bipolar reduction and the use of scrapers and backed tools in lower Bed V, and noted that the artefacts obtained from the immediately underlying MSA deposits in Bed VI-A did not have these characteristics. Diez-Martín et al. (2009) also documented some other differences within the Bed V assemblage: namely, the larger percentage of freehand technology in lower and middle Bed V, the much higher proportion of standardised geometric (e.g., crescents) and non-geometric microlithics in upper Bed V, and the presence of symbolic objects (three OES beads and nine ochre fragments) in upper Bed V. They considered these differences insufficient, however, to justify dividing the Bed V assemblage into two different industries. Instead, based on both the technology and typology of the assemblage, Diez-Martín et al. (2009) considered the artefacts in Bed V to be more appropriately defined as LSA.

The basal few centimetres of Unit C consist of very fine-grained loamy sands with rock fragments and bones attached or cemented by algal carbonates, suggestive of a higher lake level that may have submerged the site (Prendergast et al., 2007). This layer corresponds to Mehlman's Bed IV and is culturally sterile. The remainder of Unit C and the overlying Units B and A are collectively equivalent to Bed III, and contain evidence for LSA occupation. Mehlman divided Bed III into lower, middle and upper sections to define the archaeological industries. Lower Bed III is associated with the Naseran Industry, an early LSA tradition characterised by a rarity of points and backed pieces (Mehlman, 1989). The lower Bed III assemblage studied by Mehlman also contained large quantities of OES fragments and beads, and several bored stone balls. By contrast, the equivalent assemblage collected in 2005 contained abundant microlithics, including crescents, across the entire Bed III sequence, with a continuation of the components found in Bed V (Diez-Martín et al., 2009). Stone knives are also a common feature of this assemblage.

Mehlman (1989) recognised an aceramic LSA in the middle section of Bed III, but it was not well defined because of a small sample size. He also noted a reduced abundance of geometric microlithics and a higher frequency of curve-backed pieces. A ceramic LSA, known as the Oldeani Industry, appears in upper Bed III, along with a profusion of backed microlithics. The ceramics include Kansyore ware, an LSA ware traditionally associated with hunter-gatherers, as well as Narosura and Lelesu wares, which were produced by pastoral Neolithic and Iron Age people, respectively. These wares have previously been found together in secure stratigraphic contexts, with no evidence of post-depositional mixing, but it remains to be demonstrated if this holds true also at Mumba. Beds II and I represent more recent Iron Age deposits (Mehlman, 1989; Prendergast et al., 2007) and were not investigated in this study.

Previous chronologies

One of Mehlman's (1989) primary aims for excavating Mumba was to obtain samples for dating, and to construct a chronology for the archaeological sequence. Several of these samples were dated during the 1980s using a range of techniques, and the ages were presented in Mehlman (1989). Since then, these age estimates, along with some additional ages obtained subsequently by others, have been selectively used in the literature to support individual arguments, despite clear problems with the data set when considered in its entirety. All known age estimates for Beds III to VI at Mumba are listed in Table 1. We have omitted the two ^{14}C ages of 4860 ± 100 and 4890 ± 70 BP (Before Present) for the human burial in Bed III, as the remains may have been interred long after the time of formation of Bed III. Three features of this data set are of note.

First, the ages reported are stratigraphically inconsistent. For example, Mehlman (1989) reported four ^{230}Th/^{234}U ages for bone apatite from Bed V: one from the top, two from the middle, and one from the lower section. The two samples from the middle section gave ages that are significantly different from each other, and both are much older than the age obtained for the underlying sample (Table 1). Likewise, the ^{14}C ages for bone apatite and shells of the land snail *Achatina* from Bed V are inverted with respect to their stratigraphic positions, and samples from the same context do not have consistent ages (Table 1).

Second, most of the ages in Table 1 were obtained from samples composed of materials that are now considered less than ideal for dating and/or using sample preparation and measurement procedures that are no longer deemed reliable. These shortcomings are almost certainly responsible, in part or in whole, for the apparent age inversions and inconsistencies noted above. Uranium-series dating of bone, for example, is complicated by the variable timing and rate of uptake (and any later loss) of uranium after burial, due to the 'open system' behaviour of bone (Grün, 2006; Grün et al., 2010). At its simplest, a minimum ^{230}Th/^{234}U age can be determined by assuming that all of the uranium was absorbed by the bone soon after burial and none was lost subsequently. If U-uptake had occurred later, then the bone would be older than calculated. Some constraints can be placed on the history of uranium migration by taking advantage of the different radioactive half-lives of ^{230}Th in the ^{238}U series and ^{231}Pa in the ^{235}U series (e.g., Cheng et al., 1998). If the ^{230}Th/^{234}U and ^{231}Pa/^{235}U ages for the same sample agree within error, then it could be argued that the bone has acted as a 'closed system' after absorbing uranium. Both ages may be too young, however, if U-uptake was delayed, or too old if recent U-loss has occurred, as the daughter/parent ratios will both change in the same direction. For two of the samples from Bed V and for one sample from Bed VI-B, Mehlman (1989) reported paired ^{230}Th/^{234}U and ^{231}Pa/^{235}U ages. In each case, consistent ages were obtained from the two methods, with the ^{231}Pa/^{235}U ages being less precise due to the low natural abundance of ^{235}U. The accuracy of these ages requires verification using modern U-series methods of dating bone (Grün, 2006; Grün et al., 2010). This involves measuring uranium and thorium concentrations across sectioned

Table 1
All age estimates (in thousands of years, ka) reported in the literature for Beds III to VI at Mumba rockshelter.

Bed	Laboratory code	Uranium-series dating		Radiocarbon dating					Amino acid racemisation dating
		^{230}Th/^{234}U	^{231}Pa/^{235}U	Charcoal	Ostrich eggshell	Tufa	*Achatina* shell	Bone apatite	
III-upper	OS-61329			0.84 ± 0.08					
	AA69911			1.77 ± 0.15					
	ISGS-565			1.78 ± 0.08 (**1.53 – 1.88**)					
III-lower	ISGS-566				27.0 ± 0.8 (**30.2 – 33.4**)				
	Unknown				29 – 33				
IV	ISGS-499						36.9 ± 0.8 (**40.4 – 43.0**)		
	USGS-1505					25.1 ± 0.3 (**29.4 – 30.5**)			
V-upper	USGS-83-10	$23.7^{+1.1}_{-0.9}$							
	USGS-83-10		$23.8^{+2.5}_{-1.4}$						
	AA3299*				33.5 ± 0.9 (**36.4 – 40.6**)				
	Unknown*								45 – 65
	Unknown*								52
V-middle	USGS-82-22	$65.7^{+6.0}_{-5.4}$							
	USGS-82-33	$46.6^{+2.1}_{-1.7}$							
	GX-6622A							$29.6^{+1.4}_{-1.1}$ (**31.5 – 36.5**)	
	GX620A						>37.0 (**>41.1**)		
	ISGS-498						31.1 ± 0.5 (**34.8 – 36.5**)		
V-lower	USGS-82-20	$35.3^{+0.7}_{-0.5}$							
	USGS-82-20		$39.8^{+4.2}_{-3.8}$						
	GX6622A							21.0 ± 0.7 (**23.3 – 27.0**)	
VI-B	USGS-82-19	$131.7^{+6.9}_{-6.0}$							
	USGS-82-19		$109.5^{+44.4}_{-23.0}$						
	GX-6623A							19.8 ± 0.8 (**21.6 – 25.6**)	

The uncalibrated radiocarbon ages are listed for all samples, except the youngest pair in Bed III-upper, which were published as calibrated ages by Prendergast et al. (2007), who used the IntCal04 calibration curve (Reimer et al., 2004). For the other samples, we used the updated IntCal09 curve (Reimer et al., 2009) and the calibrated age ranges (at 2σ) are shown in bold. The exact provenance in Bed V of the three samples marked with an asterisk is not known.

pieces of bone to obtain profiles that can be compared with those generated by models of uranium diffusion and adsorption (e.g., Pike et al., 2002). Reliable ages can be determined only for bones with certain profiles, and this may occur in a minority of cases.

The situation is no better as regards the ^{14}C chronology for Mumba. Mehlman (1989) obtained ^{14}C ages from six different materials: charcoal, snail shell, ostrich eggshell, bone collagen, bone apatite and tufa. For each type of sample material, the ^{14}C related to the target event must first be separated from any older or younger ^{14}C using appropriate pretreatment procedures. This is likely to be problematic for many of the materials used to obtain ^{14}C ages for Beds IV, V and VI. For example, bone apatite (the mineral component of the bone) and shells often give erroneous ages due to carbon exchange with the carbonate in the apatite and shell structure during diagenesis (Taylor, 1987; Stafford et al., 1991; Hedges and van Klinken, 1992; Surovell, 2000; Bronk Ramsey, 2008). The environmental conditions at Mumba are conducive to carbon exchange in such materials, given the evidence for post-depositional formation of secondary carbonates in the form of carbonate nodules throughout the deposit and carbonate concretions around the bones, shells and stones (Prendergast et al., 2007). Thicker shells are generally preferred for ^{14}C dating, so that the exterior can be removed and the unaltered aragonite crystals isolated for analysis. However, *Achatina* shells are fragile and thin-walled, so it is unlikely that this precaution was taken. Sample preparation procedures for bone, eggshell and small land-snail shells have improved greatly in the last decade (Bird et al., 2003; Bronk Ramsey, 2008) and have been shown to increase the accuracy of the resulting ^{14}C ages, especially after molecular ultrafiltration of bone collagen (Bronk Ramsey et al., 2004; Higham et al., 2006). None of the ^{14}C ages at Mumba were obtained using these procedures, however, so they should conservatively be regarded as potentially unreliable.

The third feature of the existing chronology for Mumba is the recent proliferation in the literature of ages published without any associated estimates of uncertainty or supporting information to justify their reliability. This includes accelerator mass spectrometry ^{14}C ages of between ~29 and 33 ka (Conard, 2005) and AAR ages of about 52 ka and 45–65 ka (McBrearty and Brooks, 2000) for ostrich eggshell. Furthermore, ^{14}C ages are commonly used to calibrate the rate of AAR in eggshell, so the questionable validity of the ^{14}C ages at Mumba compromises the accuracy of the published AAR ages. It is not feasible to make an informed scientific assessment of the reliability of these chronological claims without adequate contextual and methodological information or accompanying estimates of precision.

OSL dating

Background

OSL dating is a technique used to determine the burial age of sediments (Huntley et al., 1985; Aitken, 1998). When grains of quartz or feldspar are exposed to sunlight, electrons are released from light-sensitive traps in the crystal lattice and the OSL 'clock' is reset. Once the grains are buried and hidden from daylight, they are exposed to ionising radiation from the radioactive decay of ^{238}U, ^{235}U, ^{232}Th (and their daughter products), ^{40}K and ^{87}Rb in the surrounding deposits, as well as from cosmic rays. Absorption of this radiation energy results in electron traps being refilled gradually over time. The rate of supply of radiation energy to the grains is known as the environmental dose rate. When the grains are illuminated in the laboratory using light-emitting diodes (LEDs) or a laser beam, the light-sensitive traps are again emptied of their electrons and some of these give rise to the emission of OSL. By comparing these so-called 'natural' OSL intensities with those measured after the grains have been given a known radiation dose in the laboratory, it is possible to estimate the equivalent dose (D_e) absorbed by the grains since they were last bleached by sunlight (Fig. 4). The burial age of grains that were well-bleached at the time of deposition can then be calculated by dividing the D_e by the estimated dose rate for the entire period of burial. OSL ages are obtained in calendar years, so they are directly comparable to ^{230}Th/^{234}U and ^{231}Pa/^{235}U ages and to calibrated ^{14}C ages.

Sample collection

Quartz and feldspar grains from volcanic provinces are known to pose a variety of problems for luminescence dating (Fattahi and Stokes, 2003; Tsukamoto et al., 2003; Westaway and Roberts, 2006). In the East African Rift Valley, some samples of quartz have proven challenging for dating because of their undesirable OSL properties (e.g., Choi et al., 2006), whereas other samples of quartz, and mineral mixtures dominated by the luminescence emissions from feldspars, have been used to investigate the soil erosion history and Pastoral Neolithic settlement of Tanzania and Kenya (Eriksson et al., 2000; Wright et al., 2007). The Mumba deposits are predominantly derived from metamorphic and not volcanic sources, so in June 2007 we collected 16 sediment samples to assess the suitability of the quartz and potassium (K) feldspar grains for OSL dating. The approximate positions of 15 of these samples are shown as filled circles in Fig. 2d. One sample was also collected from the Köhl-Larsen spoil heap to the west of the rockshelter.

Two of the OSL samples were collected from the northern section wall, but the majority of samples were collected from Trench 5 (n = 5) and Trench 7 (n = 8), which were excavated originally in 2005. Both trenches were 2 × 2 m in plan area with maximum depths of 2.63 m and 0.92 m, respectively. Trench 5 spans Units A–C of Prendergast et al. (2007), equivalent to Beds I–III of Mehlman (1989) and ending at the boundary of Beds III and IV. Trench 7 includes the base of Unit C and all of Units D–G, which correspond to Mehlman's (1989) Beds IV, V and VI-A. In this paper, we present and discuss results for eight samples collected from Units C–G, which cover the time interval of interest; the other eight samples remain unopened. Photographs of the locations of the eight dated samples are shown in Fig. 2a and b and are plotted in

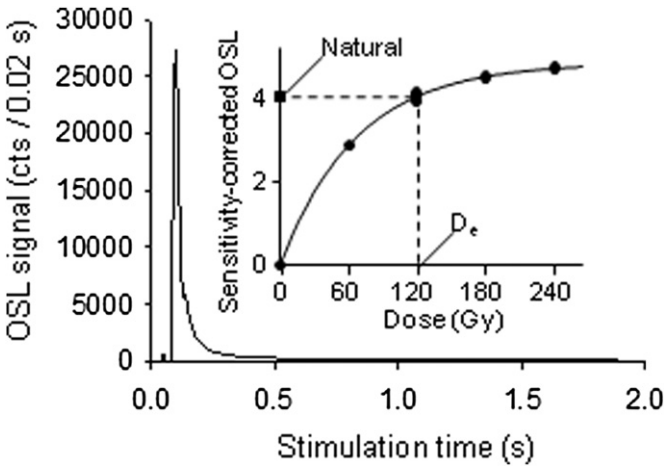

Figure 4. Natural OSL decay curve and sensitivity-corrected dose–response curve (inset) for a single grain of quartz from Mumba rockshelter. The sensitivity-corrected natural signal is projected onto the dose–response curve to estimate the equivalent dose (D_e) by interpolation. The OSL characteristics of this grain are typical of those exhibited by grains accepted for age determination.

stratigraphic context in the section drawing below (Fig. 2d). Table 2 lists the geological units of Prendergast et al. (2007) from which these samples were collected, and the equivalent stratigraphic and archaeological contexts of Mehlman (1989).

All samples were collected at night using only dim, red-filtered torchlight for illumination. Due to the presence of large rocks in the deposit, it was not practicable to obtain samples by hammering plastic tubes into the cleaned section faces. Instead, we made narrow slots and small-diameter holes in the deposit using trowels and an auger, and collected the excavated sediment in plastic bags that were immediately wrapped in black plastic for protection from light and for transport to the laboratory. The resulting slots and holes were large enough to permit in situ gamma spectrometry measurements at each sample location. Also, separate bags of sediment were collected for laboratory measurements of environmental radioactivity and sample moisture content.

Preparation and measurement procedures

Samples were prepared using standard methods (Aitken, 1985; Wintle, 1997). Carbonates were dissolved using 10% and then 32% hydrochloric (HCl) acid, and organic matter was oxidised in 10% and then 50% hydrogen peroxide (H_2O_2) solution. The residue was then dry sieved to separate the 180–212 μm diameter grain-size fraction. Quartz grains were isolated using sodium polytungstate solutions with specific gravities of 2.70 to remove heavy minerals and 2.62 to remove feldspars. The latter were separated into potassium- and sodium-dominated fractions using a solution with a specific gravity of 2.58. The quartz grains were etched in 40% hydrofluoric (HF) acid for 45 min to dissolve the external rind irradiated by alpha particles (~9 μm thick) and to destroy any remaining feldspars. The separated K-feldspar grains were etched in 10% HF acid for 10 min to remove the alpha-irradiated rinds. The etched quartz and K-feldspar grains were then washed with 32% HCl acid for 45 min to remove any precipitated fluorides, and finally re-sieved to obtain the 180–212 μm grain-size fraction for dating.

All luminescence measurements were made using two automated Risø TL/OSL readers, one of which was fitted with a laser attachment for single grain dating (Bøtter-Jensen et al., 2003). Laboratory irradiations were given using calibrated $^{90}Sr/^{90}Y$ beta sources, mounted on both readers. A focussed green (532 nm) laser beam was used to stimulate individual quartz grains for 2 s at 125 °C and the ultraviolet OSL emissions were detected by an Electron Tubes Ltd. 9235QA photomultiplier tube fitted with two 3 mm-thick Hoya U-340 filters. The same photomultiplier tube was fitted with Schott BG39 and Corning 7–59 filters to detect the blue emissions from multi-grain aliquots of K-feldspar when stimulated by infrared (875 nm) LEDs for 100 s at 50 °C and then at 225 °C, with the latter infrared stimulated luminescence (IRSL) signal used for dating.

For both quartz and K-feldspar grains, the D_e was estimated using a single-aliquot regenerative-dose (SAR) procedure to construct a dose–response curve and determine the D_e by interpolation of the natural signal (Galbraith et al., 1999; Murray and Wintle, 2000). In this procedure, after the natural and regenerative dose OSL and IRSL signals have been measured for each grain of quartz or aliquot of K-feldspar, a small 'test' dose of fixed size is given and the induced OSL and IRSL signals are measured. The test dose signals are used to monitor and correct for any sensitivity changes that commonly occur in mineral grains due to them being repeatedly dosed, heated and illuminated as part of the SAR procedure. The natural and regenerative dose signals are divided by the corresponding test dose signals to produce a set of 'sensitivity corrected' values from which the D_e is estimated. Before measuring the natural, regenerative and test dose signals, each grain or aliquot is heated to between 160 °C and 280 °C for a few seconds. The temperature and duration of these 'preheats' are optimised for each sample (or a set of related samples) by performing a series of routine tests. These include a dose recovery test on grains that are bleached in the sun and then given a known laboratory dose, to verify that the correct (given) dose can be obtained using the chosen measurement conditions (Galbraith et al., 1999). For the quartz samples from Mumba, a high-temperature optical stimulation was included at the end of the natural and each regenerative dose cycle to reduce the progressive build-up of electronic charge in the less light-sensitive traps (Murray and Wintle, 2003; Jacobs et al., 2006c). For the K-feldspar samples, we used the elevated temperature (225 °C) IRSL signal (Thomsen et al., 2008) for dating, following the post-IR IRSL procedure of Buylaert et al. (2009). Full details of these procedures and the specific experimental conditions used to measure the quartz and K-feldspar grains are described in Gliganic et al. (2012), together with their luminescence characteristics and the data analysis methods used to estimate their D_e values.

Equivalent dose (D_e) distributions

We measured the D_e values for both quartz and K-feldspar to exploit the advantages of each mineral and to help overcome their specific limitations. One of the most important advantages of single grain measurements of quartz is the ability to identify and eliminate individual grains that exhibit aberrant luminescence characteristics, as these can lead to erroneous D_e estimates when grains are combined on a multi-grain aliquot (Jacobs and Roberts, 2007). Between 600 and 1700 individual grains of quartz were measured for each of the Mumba samples (Table 3). Measurement and characterisation of the signal for each grain revealed large variability in the OSL response of grains from the same sample (Gliganic et al., 2012). For each sample, grains with aberrant luminescence characteristics were identified and then discarded from the data set, using a set of standard and tested criteria (e.g., Jacobs et al., 2006a). Of particular concern for the Mumba samples were the problems associated with the early onset of dose saturation in many of the quartz grains, which could place a major restriction on the reliable

Table 2
OSL samples from Mumba rockshelter dated in this study.

Sample code	Excavation trench	Depth below surface (cm)	Geological unit	Stratigraphic context	Archaeological context
MR2	5	40	C-upper	III upper	LSA
MR3	5	75	C-upper	III middle	LSA
MR4	5	155	C-lower	III lower	Nasera Industry
MR6	7	248	E-upper	V upper	Mumba Industry
MR7	7	288	E-middle	V middle	Mumba Industry
MR8	7	316	E-lower	V lower	Mumba Industry
MR9	7	350	G-upper	VI-A upper	Kisele Industry
MR10	7	405	G-lower	VI-A middle	Kisele Industry

The collection location, burial depth, geological unit (Prendergast et al., 2007) and stratigraphic and archaeological contexts (Mehlman, 1989) are indicated for each sample.

determination of D_e. This problem was further exacerbated by the relatively high environmental dose rates that also increased with sample depth (Table 4). In a controlled laboratory experiment on samples with D_e values $\geq$100 Gy, we found that erroneous D_e values were obtained from individual grains that had characteristic saturation doses (D_0 values) of <25 Gy (Gliganic et al., 2012). So, in addition to the standard rejection criteria, we also excluded all such grains. This restricted our data sets to grains that exhibited reliable quartz OSL characteristics (e.g., the rapid decay of signal with stimulation time, indicative of grains dominated by the 'fast' component of quartz OSL, and dose–response curves that could be fitted with a single saturating exponential function). Fig. 4 shows typical OSL decay and dose–response curves for a single grain included in the final data set. Gliganic et al. (2012) provide a full report on the OSL signal characteristics of individual quartz grains, the categories of grain behaviour, and the rejection criteria applied to the Mumba samples.

In addition to the removal of grains with aberrant luminescence behaviours, analysis of individual grains of quartz has further benefits in archaeological contexts where: 1) post-depositional disturbances (Feathers et al., 2006, 2010; Jacobs et al., 2006b, 2008b; David et al., 2007), 2) the effects of beta microdosimetry (e.g., Jacobs et al., 2008c), and 3) the possibility of roof spall contamination and other forms of non-homogeneous bleaching (Roberts et al., 1998, 1999; Jacobs et al., 2011) are of concern (Jacobs and Roberts, 2007). The archaeological sediments at Mumba rockshelter show potential for, at least, the first two major concerns. Between 20 (MR10) and 106 (MR3) grains (3.3–8.8% of the measured grains) were accepted for D_e determination, with the resulting distributions having overdispersion values of between 29 $\pm$ 4 and 73 $\pm$ 6% (Table 3). Overdispersion refers to the spread remaining among D_e estimates after taking the measurement errors into account. It is common for single grain D_e distributions to be overdispersed by 10–20%, even if all grains had been fully bleached before burial and had subsequently remained undisturbed and exposed to the same dose rate (Jacobs and Roberts, 2007). But the distributions of accepted D_e values are more dispersed still for the Mumba samples, and can be divided into three broad types, displayed as radial plots for three representative samples in Fig. 5. Radial plots for all the samples are provided as Figure S1 in SOM and in Gliganic et al. (2012).

The first type of D_e distribution (Fig. 5a) was only found for MR2 (stratigraphically the highest sample) and is representative of a sediment sample that has been continuously exposed to light as a result of anthropogenic processes (such as digging) or natural processes (such as animal burrowing or bioturbation). Prendergast et al. (2007) reported a variety of features indicative of anthropogenic disturbance of the upper layers by digging. The radial plot for MR2 shows no discrete dose components and the D_e values could not be combined in any meaningful way to obtain a single representative D_e value for final age determination. Instead, we calculated the minimum and maximum D_e values for this sample using the minimum age model of Galbraith et al. (1999) and the maximum age model of Olley et al. (2006), respectively, to obtain an age range. The stratigraphic integrity of artefacts found within this layer cannot be assured.

The second type of D_e distribution was found for two of the samples, MR3 and MR9, which consisted of four and three discrete dose components, respectively, and are referred to here as 'mixed' D_e distributions (Fig. 5b). The finite mixture model (FMM) of Roberts et al. (2000) was used to obtain the weighted mean D_e value of each dose component and the proportion of grains in each of them, following the procedures described by David et al. (2007) and Jacobs et al. (2008b, 2011). For both samples, the dominant dose component, represented by the greatest proportion of the grains, was used in the final age calculation. The degree of mixing is relatively small, with only 7 and 16% of the grains being intrusive in MR3 and MR9, respectively. Large-scale movement of grains, and hence artefacts, is unlikely to result in such limited mixing, suggesting that all artefacts in these layers are likely to be in primary position.

The third type of D_e distribution is representative of the remainder of the samples, and also MR3 and MR9 after removal of the grains identified as being intrusive. These D_e distributions showed either a dominant single component with several smaller D_e values (e.g., MR7; Fig. 5c) or two discrete dose components in approximately equal proportion (e.g., MR6). We refer to both types as 'scattered' D_e distributions, using the nomenclature of Jacobs et al. (2008b). The FMM was applied to these samples in the same way as the 'mixed' D_e distributions and the dose components containing the largest proportion of grains were used for final age determination. For all these samples, the presence of the additional low dose component was attributed to small-scale differences in the beta dose received by individual grains. Small carbonate nodules are abundant in geological units C, D and E (Fig. 3) and all artefacts, bones and shells are heavily concreted in carbonate (Prendergast et al., 2007). Carbonates are generally much less radioactive than the detrital grains they abut or surround, resulting

Table 3
Summary table of results for individual grains of quartz and multi-grain aliquots of K-feldspar.

Sample code	Mineral	No. of grains or aliquots measured	No. of grains or aliquots accepted	D_e overdispersion (%)	Age model	Final D_e (Gy)
MR2	Quartz	1200	78	73 $\pm$ 6	Min	2.3 $\pm$ 0.3
					Max	31.3 $\pm$ 4.1
MR3	Quartz	1200	106	52 $\pm$ 4	FMM	39.1 $\pm$ 2.2
	Feldspar	24	24	51 $\pm$ 7	CAM	51.4 $\pm$ 5.3
MR4	Quartz	900	46	35 $\pm$ 5	FMM	95.1 $\pm$ 7.2
MR6	Quartz	1700	67	29 $\pm$ 4	FMM	153.3 $\pm$ 11.3
	Feldspar	24	24	19 $\pm$ 3	CAM	150.9 $\pm$ 5.8
MR7	Quartz	1300	48	40 $\pm$ 6	FMM	143.3 $\pm$ 8.5
MR8	Quartz	1500	81	47 $\pm$ 5	FMM	173.3 $\pm$ 11.5
MR9	Quartz	1500	84	59 $\pm$ 6	FMM	216.9 $\pm$ 16.5
	Feldspar	24	22	22 $\pm$ 3	CAM	190.8 $\pm$ 9.2
MR10	Quartz	600	20	34 $\pm$ 9	FMM	160.3 $\pm$ 34.9
	Feldspar	24	23	23 $\pm$ 3	CAM	258.1 $\pm$ 12.5

The numbers of grains or aliquots measured and accepted (after application of the rejection criteria described in Gliganic et al., 2012) are listed, along with the overdispersion estimates for the D_e values of accepted grains or aliquots. Also shown are the statistical age models used to calculate the final D_e values for age determination—central age model (CAM, also used to estimate D_e overdispersion), finite mixture model (FMM), minimum age model (Min) and maximum age model (Max)—and the D_e values so obtained.

Table 4
Environmental dose rates and supporting data for quartz and K-feldspar separates.

Sample code	External dose rate (Gy/ka)			Internal dose rate (Gy/ka)		Total dose rate (Gy/ka)		
	Beta	Gamma	Cosmic	Quartz	Feldspar	Bulk quartz	Beta-adjusted quartz	Bulk feldspar
MR2	1.50 ± 0.09	0.98 ± 0.03	0.10	0.03	0.90	2.61 ± 0.12	–	–
MR3	1.22 ± 0.08	0.93 ± 0.02	0.09	0.03	0.90	2.28 ± 0.11	2.51 ± 0.12	3.15 ± 0.12
MR4	1.27 ± 0.07	0.71 ± 0.02	0.09	0.03	0.90	2.11 ± 0.10	2.58 ± 0.12	–
MR6	1.35 ± 0.07	1.04 ± 0.03	0.08	0.03	0.90	2.50 ± 0.11	3.12 ± 0.14	3.37 ± 0.12
MR7	1.58 ± 0.08	0.92 ± 0.02	0.08	0.03	0.90	2.62 ± 0.12	2.79 ± 0.14	–
MR8	1.54 ± 0.08	0.91 ± 0.02	0.08	0.03	0.90	2.57 ± 0.12	3.04 ± 0.14	–
MR9	1.67 ± 0.09	0.93 ± 0.02	0.08	0.03	0.90	2.71 ± 0.13	3.42 ± 0.15	3.58 ± 0.13
MR10	1.91 ± 0.10	1.00 ± 0.03	0.08	0.03	0.90	3.02 ± 0.14	3.49 ± 0.16	3.89 ± 0.15

The total dose rate represents the sum of the internal and external dose rates for each mineral (where the latter is the same for both), and the total uncertainty represents the sum (in quadrature) of the random and systematic errors. The K-feldspar ages were calculated using the bulk-sample total dose rates, whereas the quartz ages were calculated using the beta-adjusted total dose rates, which take into account the differences in beta dose rate received by individual quartz grains.

in small-scale differences in the beta dose rate delivered to individual quartz grains (e.g., Jacobs et al., 2008c). An adjustment to the beta dose rate measured in the laboratory is thus required, as discussed in the next section.

Table 3 provides a summary of the number of grains measured and accepted for each sample, the overdispersion values of the D_e distributions, and the age models and final D_e values used to calculate the burial ages. Further details are presented in Gliganic et al. (2012).

The most important advantage of K-feldspar over quartz as a dosimeter is its much higher dose saturation limit, which should make it practicable to measure much larger burial doses and, hence, date older samples. K-feldspars also have a much greater contribution to the dose rate from radioactive potassium (^{40}K), rubidium (^{87}Rb), uranium and thorium within the mineral grains. This internal component of the dose rate is not affected by the inhomogeneous distribution of radioactivity external to the grains, thus reducing the effect that small-scale variations in the beta dose rate may have on the spread in D_e values; a problem that was common to all of the quartz measurements. But our chief concern with the quartz data sets, especially for the older samples, was the proximity of the D_e values to the dose saturation limit, which may result in age underestimation. To test this possibility, 24 aliquots, each containing ~50 feldspar grains, were also measured for four of the eight samples (MR3, MR6, MR9 and MR10) using a post-IR IRSL measurement procedure (Thomsen et al., 2008; Buylaert et al., 2009), described in detail by Gliganic et al. (2012). Because the feldspars were measured as multi-grain aliquots and not as individual grains, it is not appropriate to fit the FMM to the resulting D_e distribution (Arnold and Roberts, 2009). Instead, we calculated the weighted mean D_e value for each of the samples using the central age model (CAM) of Galbraith et al. (1999), but recognise that the CAM values for MR3 and MR9 may be distorted by the inclusion of D_e estimates for intrusive grains.

Overdispersion values of between 19 ± 3 and 23 ± 3% were calculated for the D_e distributions of samples MR6, MR9 and MR10, and 51 ± 7% for MR3. Single grain quartz D_e measurements of the latter sample showed evidence for some post-depositional mixing, which would account for the unexpectedly large spread in D_e values among the feldspar aliquots. The D_e and overdispersion values are listed in Table 3, and a representative D_e distribution (MR6) is plotted in Fig. 6. The radial plots for the remaining samples are provided as Figure S2 in SOM and in Gliganic et al. (2012). For feldspars, the measured D_e is commonly underestimated because of the ubiquitous and malign phenomenon of anomalous fading (Wintle, 1973). A correction for fading must be made to obtain an accurate estimate of burial age, and we used the correction method of Huntley and Lamothe (2001). The reliability of this correction was tested and confirmed by comparing the K-feldspar and quartz ages (see below).

Environmental dose rates

The total environmental dose rate to sand-sized etched grains of quartz and feldspar consists of contributions from beta, gamma and cosmic radiation external to the grains, plus an internal dose rate due to radioactive inclusions (Table 4). Both minerals receive a small internal alpha dose from U and Th inclusions, while K-feldspar grains also receive a significant internal beta dose from the radioactive decay of ^{40}K and ^{87}Rb. To estimate the dose rates for the Mumba samples, laboratory measurements of radioactivity and water content were made using separate bags of sediment collected from each of the OSL sample locations.

The external beta dose rates were determined by grinding a dried portion of each sample to a fine powder and measuring the total beta counts using a Risø GM-25-5 beta counter (Bøtter-Jensen and Mejdahl, 1988). Allowance was made for beta-dose attenuation due to grain size and HF acid etching (Mejdahl, 1979). For the quartz samples, we also adjusted the beta dose rate to compensate for the inhomogeneous distribution of radionuclides adjacent to some of the grains. The adjustment was based on the relative proportion of grains assigned by the FMM to the main D_e component of each sample (except MR2), following Jacobs et al. (2008c, 2011). Table 4 lists the beta-adjusted total dose rates used to calculate the quartz ages, along with the unadjusted total dose rates for the bulk samples. This adjustment procedure is not applicable to the D_e values obtained from multi-grain aliquots of K-feldspar, for which burial ages were calculated using the bulk-sample total dose rates.

The gamma dose rates were measured by in situ gamma spectrometry at each sample location. The combined gamma dose rate from the ^{238}U and ^{232}Th decay chains and from ^{40}K was determined using the 'threshold' technique (Mercier and Falguéres, 2007), with the spectrometer calibrated using the doped concrete blocks at Oxford (Rhodes and Schwenninger, 2007). Such measurements take account of any spatial heterogeneity in the gamma radiation field surrounding each OSL sample.

A small, internal alpha dose rate of 0.03 ± 0.01 Gy/ka was assumed for the quartz grains of all samples, based on measurements made on South African quartz (Jacobs et al., 2006b). For the K-feldspars, an internal beta dose rate was calculated by assuming internal ^{40}K and ^{87}Rb concentrations of 12.5 ± 0.5% (Huntley and Baril, 1997) and 400 ± 100 μg/g (Huntley and Hancock, 2001), respectively. These were converted to dose rates using the conversion factors of Adamiec and Aitken (1998), and corrected for the absorbed dose fraction. For K-feldspar grains of 180–212 μm diameter, this yields an effective internal beta dose rate of 0.80 ± 0.03 Gy/ka, to which we added 0.10 ± 0.03 Gy/ka for the effective internal alpha dose rate from U and Th inclusions.

The cosmic-ray dose rates were estimated from the equations provided by Prescott and Hutton (1994), taking into account the burial depth of each sample (averaged over the entire period of

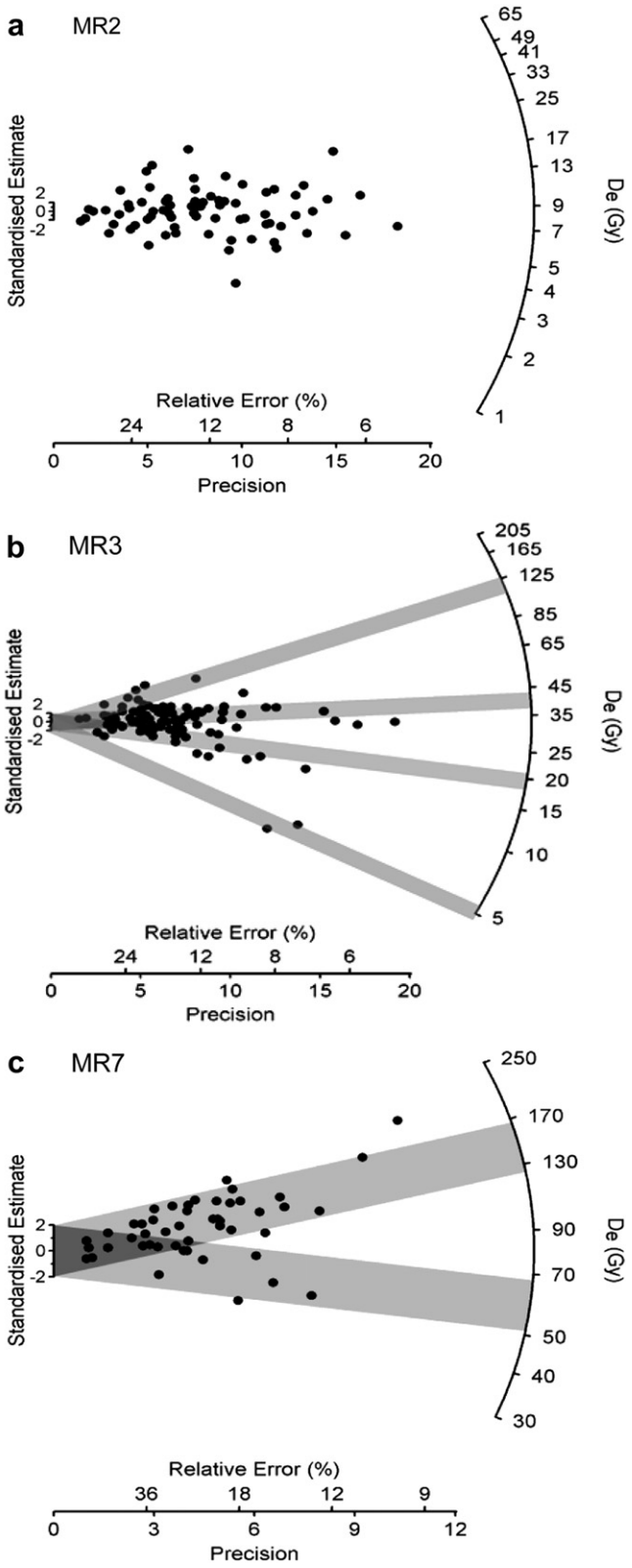

Figure 5. Radial plots of single grain D_e distributions for three quartz samples. Each point shows the D_e value and measurement error for an individual grain. The D_e is the point of intersection on the radial axis of a line projected from the origin on the left-hand axis through the data point of interest. The relative error on this D_e is read off the x-axis by extending a vertical line from the data point, so the most precise D_e estimates fall furthest to the right. a. The D_e distribution for MR2 shows no evidence for discrete dose components. b. and c. The distributions for MR3 and MR7 are categorised as 'mixed' and 'scattered', respectively, and were fitted using the finite mixture model. The fitted components are indicated by grey bands, which are centred on the weighted mean D_e value for each component.

burial), the density of sediment overburden, and the altitude and geomagnetic latitude of Mumba rockshelter. We also took into consideration the $\cos^2 \Phi$-zenith angular distribution of cosmic rays to allow for the extent of rock shielding of the deposit (Smith et al., 1997).

The total dose rates and supporting information are summarised in Table 4. We assume that the measured radionuclide concentrations and dose rates have prevailed throughout the period of sample burial, but note that the methods used to measure the beta and gamma dose rates in this study are not likely to be compromised by U-series disequilibria (Olley et al., 1996, 1997). For all samples, a water content of $10 \pm 2\%$ (mass of water as a percentage of the mass of dry sample) was used in conjunction with dose rate correction factors (Aitken, 1985; Readhead, 1987) to calculate the external beta, gamma and cosmic-ray dose rates. For the latter, this correction was applied only to the cosmic rays penetrating the sediment overburden. This water content is moister than the measured (field) values of 3.3–8.2% to allow for past fluctuations in lake level and drying out of the section faces after excavation. The calculated burial ages increase by ~1% for each 1% increase in water content, as interstitial pore water absorbs radiation that would otherwise have reached the grains.

Quartz and K-feldspar ages

The final ages derived from the single grains of quartz and multi-grain aliquots of K-feldspar are presented in Table 5. Where a sample was measured using both minerals, the ages are statistically consistent within one standard error, except for MR10. This provides confidence in the measurement and analysis of their luminescence signals and environmental dose rates, and suggests that the fading correction applied to the feldspar aliquots, and the beta dose adjustment made for the quartz grains, are likely appropriate. However, the quartz ages are similar whether calculated from the CAM estimates of D_e and bulk-sample dose rates or from the FMM estimates of D_e and beta-adjusted dose rates (Gliganic et al., 2012), but the latter takes account of the presence of intrusive grains and secondary carbonates. The feldspar ages are similarly insensitive to the fading correction, owing to the selection of the post-IR IRSL signal for dating (Gliganic et al., 2012), but we consider the single grain quartz ages to be more accurate because intrusive grains could be identified and excluded prior to age calculation.

The sole exception is MR10, for which the feldspar age is preferred. For this sample, the natural OSL signals for the 20 individual quartz grains from which D_e values could be obtained lay very close to the saturation intensity. While the small number of grains in the quartz data set may have resulted in the age underestimation, we think that these finite D_e values may constitute only the leading edge of the D_e distribution and, thus, represent a minimum D_e value for MR10. This notion is further supported by the large associated uncertainty on the quartz age for this sample and the apparent age inversion relative to samples from stratigraphically younger deposits. It was for this reason that we decided to investigate and measure K-feldspar grains to extend the luminescence chronology to the older archaeological deposits at Mumba.

The single grain quartz ages for samples MR2-4 and MR6-9, and the K-feldspar age of sample MR10, are in correct stratigraphic order (Table 5). The deepest dated deposits (Bed VI-A), corresponding to the Kisele Industry, are 73.6 ± 3.8 ka in age (MR10). The

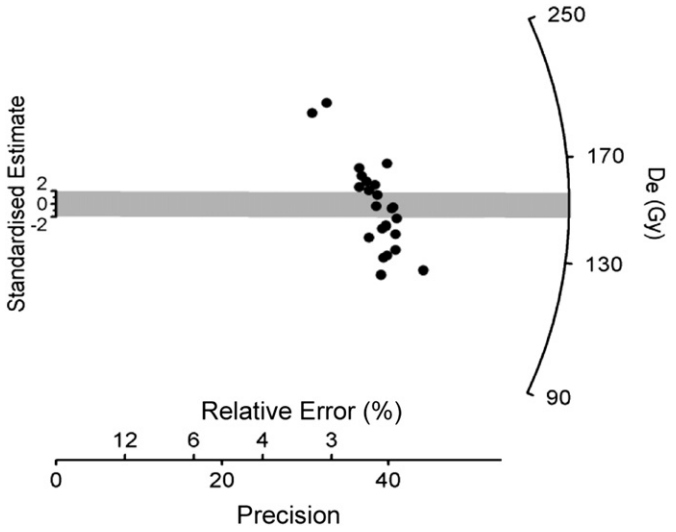

Figure 6. Radial plot of the D_e values obtained for 24 multi-grain aliquots of K-feldspar from sample MR6.

upper portion of Bed VI-A is dated to 63.4 ± 5.7 ka (MR9) and the lower part of Bed V, which contains the earliest evidence for the Mumba Industry, was deposited 56.9 ± 4.8 ka ago (MR8). Thus, the transition between the Kisele and Mumba Industries occurred at ~60 ka. The upper section of Bed V, which contains the oldest OES beads and the highest proportion of microlithics associated with the Mumba Industry (Diez-Martín et al., 2009), is dated to 49.1 ± 4.3 ka (MR6). The OSL chronology suggests, therefore, that the Mumba Industry persisted for 7.8 ± 6.3 ka and may have ended as late as 40 ka ago. Ages of 36.8 ± 3.4 ka (MR4) and 15.6 ± 1.2 ka (MR3) were obtained for the lower and middle sections of Bed III, with the former associated with the Naseran Industry (Mehlman, 1989). We were unable to determine a single depositional age for upper Bed III, as the single grain D_e distribution for this sample (MR2) is consistent with substantial and continuous sediment mixing (Fig. 5a). The minimum and maximum age estimates for MR2 are 0.84 ± 0.16 and 12.0 ± 1.7 ka. This age range indicates that these sediments have been extensively disturbed since initial deposition, with the oldest grains exposed to sunlight more recently than the vast majority of grains in MR3.

The internally consistent luminescence chronology developed in this study for Mumba rockshelter contrasts with the lack of stratigraphic coherence exhibited by previous chronologies for the site (Table 1). For example, previous age estimates for Bed V range from ~23 to 66 ka and show no coherent relation of age with depth, whereas the OSL ages progressively increase with depth from 49.1 ± 4.3 to 56.9 ± 4.8 ka. We consider the OSL chronology to provide the most reliable timeframe for Mumba, even for the Pleistocene deposits younger than 40 ka, owing to the inadequacy of the sample preparation and measurement procedures used previously, as discussed above.

Discussion

Ideally, once a new chronology has been constructed for a site as important as Mumba, one would like to compare it with existing chronologies and to palaeoenvironmental records. Such comparisons may enable an assessment of the temporal and spatial distribution of changes in technology and behaviour, which can then be viewed in the wider context of changing climates that may shed light on why such changes may have occurred. Unfortunately, in East Africa, there is a paucity of well-dated archaeological deposits that contain comparable evidence (McBrearty and Brooks, 2000), and the Late Pleistocene climate dynamics of the region as a whole is complex and poorly understood.

Comparisons between chronologies of different sites in the region are largely futile, as most of the sites suffer from the same problems as those identified for the previous chronologies at Mumba (Table 1). That is, they have been dated more than a decade ago using sample pretreatment, measurement and analytical procedures that would now be considered inadequate, or sites have not been dated at all, or ages were obtained but supporting information to validate their reliability was not provided. The only worthwhile comparisons that can be made are with the earliest reported ages for microlithic technology in East Africa, associated with the Naisiusiu Beds in Olduvai Gorge, Tanzania, and for Enkapune Ya Muto in southern Kenya. The latter site is often claimed to contain the most convincing evidence of an early and sustained occurrence of microlithics during the Late Pleistocene (Ambrose, 2002).

Infinite ^{14}C ages of >45 ka were reported for deposits associated with the Naisiusiu Beds (Manega, 1993) and electron spin resonance (ESR) ages of 59 ± 5 ka and 62 ± 5 ka were obtained for three bovid teeth assuming early or linear uptake models of uranium, respectively (Skinner et al., 2003). The teeth were not collected in association with any artefacts, but the ESR ages are, nevertheless, consistent with the OSL age of 56.9 ± 4.8 ka for the lower Bed V deposits at Mumba, in which microlithics first occur in relatively low abundance. At Enkapune Ya Muto, the first backed artefacts (n = 3) were found in the deepest archaeological layer, which contains the Endingi Industry. The overlying Nasampolai Industry is dominated by large backed blades and geometric microlithics, several of which exhibit ochre staining on the modified edge, indicative of hafting (Ambrose, 1998, 2002). Overlying the Nasampolai is the Sakutiek Industry, which has low frequencies of

Table 5
Single grain quartz and multi-grain K-feldspar burial ages (the latter corrected for fading), together with the stratigraphic and archaeological contexts of these samples.

Sample code	Stratigraphic context	Archaeological context	Age (ka)	
			Quartz	K-feldspar (fading-corrected)
MR2	Bed III upper	LSA	0.84 ± 0.16 (Min) 12.0 ± 1.7 (Max)	–
MR3	Bed III middle	LSA	**15.6 ± 1.2**	17.9 ± 1.9
MR4	Bed III lower	Nasera Industry	**36.8 ± 3.4**	–
MR6	Bed V upper	Mumba Industry	**49.1 ± 4.3**	47.6 ± 1.8
MR7	Bed V middle	Mumba Industry	**51.3 ± 4.2**	–
MR8	Bed V lower	Mumba Industry	**56.9 ± 4.8**	–
MR9	Bed VI-A	Kisele Industry	**63.4 ± 5.7**	58.9 ± 2.6
MR10	Bed VI-A	Kisele Industry	45.9 ± 10.3	**73.6 ± 3.8**

The age considered most reliable for each sample is shown in bold, with the uncertainties (including a systematic uncertainty of 2% to allow for possible bias associated with calibration of the laboratory beta source) expressed at 1σ. As explained in the text, only minimum and maximum burial age estimates are provided for MR2.

microlithics, but abundant OES beads ($n = 13$), bead platforms ($n = 12$) and fragments ($n = 593$).

The chronology reported for Enkapune Ya Muto consists of obsidian hydration and uncalibrated ^{14}C ages, the latter obtained from charcoal and OES. An uncalibrated ^{14}C age on charcoal of 41.4 ± 0.7 ka BP was reported for the Endingi Industry. No ^{14}C ages were obtained for the important Nasampolai Industry, but four ages on charcoal and OES of 29.3 ± 0.8, 35.8 ± 0.6, 37.0 ± 1.1 and 39.9 ± 1.6 ka BP were reported for the Sakutiek Industry. These ages are in correct stratigraphic order and, when calibrated, range from ~45 cal ka BP (Endingi) to ~44–41 cal ka BP (Sakutiek) if the youngest age is omitted, as proposed by Ambrose (1998). Obsidian hydration ages of 32.5 ± 1.2 ka and 35.3 ± 2.2 ka were obtained for the Endingi and Sakutiek Industries, respectively, and an older age of 46.4 ± 2.8 ka for the intermediate Nasampolai Industry. Ambrose (1998) argued that the ^{14}C age for the Endingi Industry is likely a minimum age, and instead used the obsidian hydration age for the Nasampolai Industry and the uncalibrated ^{14}C ages for the overlying Sakutiek Industry to estimate sedimentation rates at the site and derive an age of 55–45 ka for the start of the Nasampolai Industry. But the obsidian hydration ages are not in stratigraphic order and those for the Endingi and Sakutiek Industries are significantly younger than their calibrated ^{14}C counterparts. Given these internal inconsistencies and the questionable reliability of the obsidian hydration dating technique as then used (Ridings, 1996; Anovitz et al., 1999), little confidence can be placed in the obsidian hydration chronology for Enkapune Ya Muto or the extrapolated starting age for the Nasampolai Industry calculated by Ambrose (1998). Consequently, it is not clear how the Enkapune Ya Muto and Mumba records are related chronologically. This example highlights the difficulties that remain in comparing the chronologies of Late Pleistocene archaeological deposits in East Africa, which are exacerbated by the uncertainties associated with the cultural attributions of, and correlations between, different assemblages.

Several researchers have also argued for a deep-seated dynamic between climate change and its effect on Pleistocene environments and human populations (e.g., Cohen et al., 2007; Scholz et al., 2007, 2011), and the possibility that the occurrence of microlithics may reflect a technological response to rapid changes in environmental conditions (e.g., Mellars, 2006; Henshilwood, 2008; Bar-Matthews et al., 2010; Mackay, 2011). In particular, proxy records of climate change in East Africa reconstructed from sediment cores collected from Lakes Malawi and Tanganyika have influenced recent ideas on human–environment interactions at a time when, and from a region where, anatomically modern humans are thought to have first exited Africa to populate the rest of the Old World (e.g., Scholz et al., 2007).

Palaeoclimatic reconstructions for East Africa are complicated, however, by the interaction of several ocean–atmosphere systems and the response of terrestrial ecosystems (e.g., Cohen et al., 2007; Scholz et al., 2007, 2011; Tierney et al., 2008, 2010, 2011). To illustrate this complexity, Fig. 7a shows the changes through time of the deuterium/hydrogen ratio of higher plant leaf waxes ($\delta D_{leaf\ wax}$), a proxy for precipitation, in sediment cores from Lakes Challa (Tierney et al., 2011) and Tanganyika (Tierney et al., 2008), while Fig. 7d shows the reconstructed lake-level elevations for Lakes Malawi (Scholz et al., 2007) and Naivasha (Richardson and Dussinger, 1986; Trauth et al., 2003; Bergner and Trauth, 2004; Bergner et al., 2009). All four lakes are situated within the East African Rift Valley (see Fig. 7b: Challa, 2; Tanganyika, 7; Malawi, 8; Naivasha, 3), but at locations that can shed light on potential longitudinal differences in hydrological response to climatic forcing. For example, Lake Malawi is located at the southern terminus of the western Rift system, whereas Lake Naivasha is located in the central part of the eastern Rift system.

It is evident that the $\delta D_{leaf\ wax}$ precipitation indices for Lakes Challa and Tanganyika are not always in phase (Fig. 7a). For example, between 25 and 19 ka (the Last Glacial Maximum, LGM), the Lake Challa values are more negative (i.e., wetter) than those at Lake Tanganyika, which represent the driest conditions of the last ~60 ka. Likewise, the lake-level records for Lakes Malawi and Naivasha (Fig. 7d) are diametrically opposed for most of the last ~140 ka. Between 75 and 15 ka (i.e., the period for which we have OSL ages at Mumba rockshelter, plotted in Fig. 7c), Lake Malawi appeared to sustain high lake levels, comparable with modern levels, whereas the levels in Lake Naivasha remained very low, except for three short periods of intermediate lake-level at ~65 ka, 27–25 ka and 19–16 ka. To further complicate the picture, Scholz et al. (2007) reported that Lakes Malawi and Tanganyika both exhibited major rises in lake level after ~70 ka, but the $\delta D_{leaf\ wax}$ precipitation index for Lake Tanganyika shows a general drying trend between 60 and 19 ka, with major lake-level fluctuations at various timescales (Tierney et al., 2008). Further, in contrast to the suggestion of Scholz et al. (2007) that Lake Malawi had high water levels during the LGM, Castañeda et al. (2007, 2009) found indications of drier conditions at this time, based on changes in molecular biomarkers and carbon isotopes in sediment cores collected from Lake Malawi.

How can we explain the differences in response of these lakes to the prevailing climatic controls, and the contrasting interpretations made for the same lake using different environmental proxies? The study of Tierney et al. (2011) sheds light on some possible reasons for the complex response of different lakes. They compared the responses of Lakes Challa and Tanganyika over the last 25 ka (Fig. 7a) to investigate the role of the winter Indian monsoon. As the latter intensifies, the trade winds increase in strength and bring more moisture on to the continent, resulting in higher precipitation. Precipitation variability at Lake Challa is influenced primarily by Indian Ocean climate dynamics, whereas Lake Tanganyika is affected not only by the latter but also by the seasonal migration of the Intertropical Convergence Zone (ITCZ, shown as solid red and green lines in Fig. 7b), and by moisture flux from the Congo basin (Tierney et al., 2010). Both lakes are located in the southern hemisphere and at approximately the same latitude, thus simplifying comparisons as much as possible. Tierney et al. (2011) attribute the differences in response of Lakes Challa and Tanganyika to the position of the Congo Air Boundary (CAB), shown as dashed red and green lines in Fig. 7b for the austral summer and winter months. The CAB is a convergence zone marking the confluence of air from the Indian Ocean with unstable air from the Congo basin. At the present day, the CAB lies well west of Lake Challa throughout the year, whereas Lakes Malawi and Tanganyika are located close to (or directly beneath, in the latter instance) the intersection of the ITCZ and CAB during the austral summer. The past hydrology of East African lakes, therefore, is likely to have been characterised by zonal gradients associated with several large-scale ocean–atmosphere systems, with the relative influx of moisture from the Indian Ocean and the Congo basin giving rise to longitudinal differences in precipitation.

Mumba rockshelter is situated southeast of Lake Eyasi (site 1 in Fig. 7b), slightly closer to Lake Challa than Lake Tanganyika and at a similar latitude. The dominant controls on Pleistocene environments are apt to have been complex, therefore, because of the location of Mumba at the intersection of several major climate systems. Given the current lack of reliable climatic reconstructions in the vicinity of Mumba, and the absence of a consensus lake-level record between 75 and 15 ka for any lake in East Africa, we consider it premature to correlate putative environmental changes with patterns of human occupation at Mumba. The same caveat applies to any archaeological record for which there is no directly

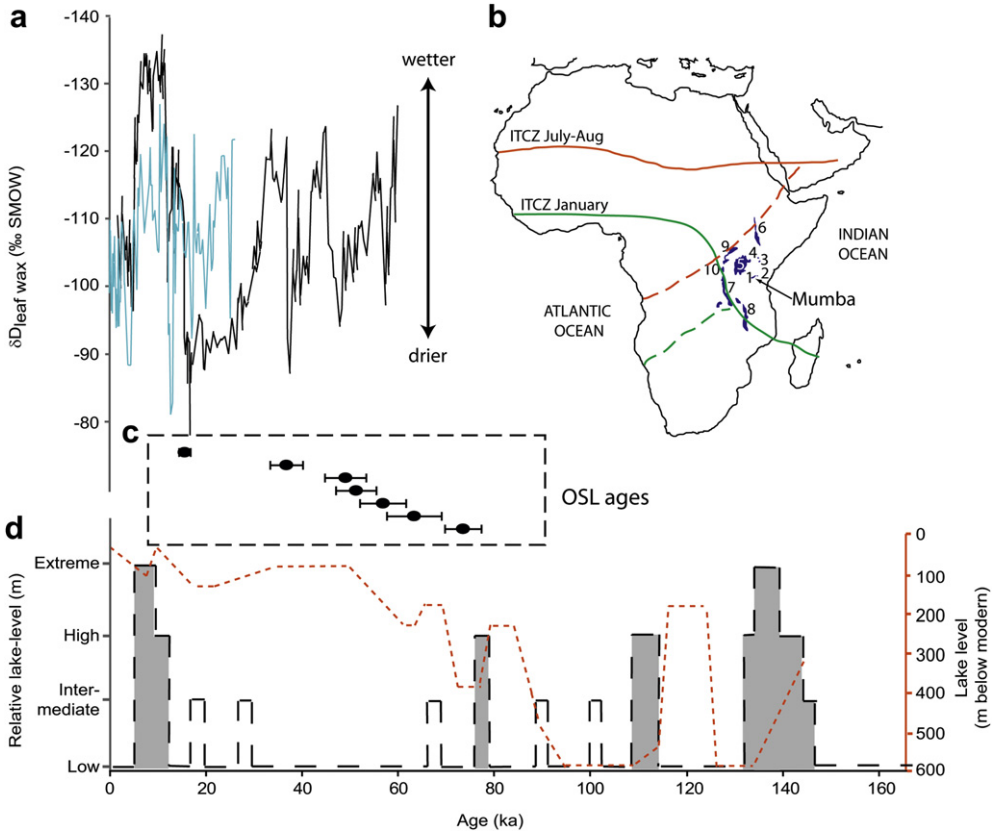

Figure 7. Summary diagram of reconstructed lake-level records for East Africa, together with OSL ages for Mumba rockshelter. a. $\delta D_{leaf\ wax}$ records for sediment cores from Lakes Challa (blue) and Tanganyika (black), used as a proxy for precipitation (Tierney et al., 2008, 2011). b. Map showing the location of Mumba in relation to Lakes Eyasi (1), Challa (2), Naivasha (3), Baringo (4), Victoria (5), Turkana (6), Tanganyika (7), Malawi (8), Albert (9) and Edward (10). The modern seasonal positions of the Intertropical Convergence Zone (ITCZ) and Congo Air Boundary are shown by solid and dashed lines, respectively. c. OSL ages for Mumba rockshelter, with total uncertainties at the 68% (1σ) confidence interval. d. Lake-level reconstructions indicated by stippled red line for Lake Malawi (Scholz et al., 2007) and black dashed line for Lake Naivasha, with periods of high to extreme water level in Lake Naivasha shaded in grey (Richardson and Dussinger, 1986; Trauth et al., 2003; Bergner and Trauth, 2004). (For interpretation of the references to color in this figure legend, the reader is referred to the web version of this article.)

associated palaeoclimatic record. Future work at Lake Eyasi or neighbouring Lake Manyara (where the Holocene sediments have been investigated; Tierney et al., 2011) may yield a coherent climatic signal that we can compare with the Mumba sequence. At this stage, however, we cannot relate the various archaeological assemblages at Mumba to particular environmental conditions, nor can we link the first appearance of microlithic technology at ~60 ka, or OES beads at ~49 ka, to specific climatic events. However, we hope that this study may provide the impetus for archaeologists, geochronologists and climate scientists to obtain archaeological and palaeoenvironmental records of much higher spatial and temporal resolution across East Africa, so that detailed regional comparisons can be made between artefact assemblages and past environments.

Conclusions

Our understanding of the MSA and early LSA in East Africa has been hindered by a lack of reliable chronologies for archaeological sequences. Here we have presented OSL ages for quartz and feldspar grains deposited at Mumba rockshelter, which provide insights into the timing of the MSA and LSA in northern Tanzania. The OSL ages are internally consistent and stratigraphically coherent, providing confidence in their reliability. The transition from pre-microlithic MSA to the microlithic Mumba Industry is constrained to ~60 ka. Single grain OSL analyses demonstrate the stratigraphic integrity of upper Bed V and lower Bed III, so the OES beads and abundant microlithics in the former are likely not intrusive and date to 49.1 ± 4.3 ka, which marks the final phase of the Mumba Industry. This would represent the earliest known occurrence of the LSA in Africa, if Diez-Martín et al. (2009) are correct in their interpretation of the Bed V Industry. Symbolic ornaments in lower Bed III proliferated 36.8 ± 3.4 ka ago in association with the Nasera Industry. At present, however, we cannot reliably compare these artefact assemblages with those excavated at other sites in the region, because of the scarcity of robust chronologies. To investigate the timing and possible drivers of technological and behavioural changes across East Africa, and place them in environmental context, requires accurate ages for additional archaeological sites and Late Pleistocene records of environmental change. Future studies, therefore, could usefully focus on the redating of other archaeological deposits in East Africa, using the same or similar OSL techniques as employed here, to help construct a common chronology for the region. Likewise, geographic and temporal coverage of the contemporaneous climatic and ecological conditions needs to be improved greatly before robust inferences about human–environment interactions can be made.

Acknowledgements

We thank the Tanzanian Commission for Science and Technology (COSTECH) and the Department of Antiquities for permission to collect OSL samples at Mumba rockshelter, and the Australian Research Council for Discovery Project DP0666084 to

Roberts and Jacobs, which funded the OSL dating program. We also thank Mary Prendergast for advice on stratigraphy and Rainer Grün for assistance with OSL sample collection, and we acknowledge the financial support of Gliganic by the University of Wollongong.

Appendix. Supplementary data

Supplementary data associated with this article can be found, in the online version, at doi:10.1016/j.jhevol.2012.02.004.

References

Adamiec, G., Aitken, M.J., 1998. Dose-rate conversion factors: update. Ancient TL 16, 37–50.

Aitken, M.J., 1985. Thermoluminescence Dating. Academic Press, London.

Aitken, M.J., 1998. An Introduction to Optical Dating: The Dating of Quaternary Sediments by the Use of Photon-stimulated Luminescence. Oxford University Press, Oxford.

Ambrose, S.H., 1998. Chronology of the Later Stone Age and food production in East Africa. J. Archaeol. Sci. 25, 377–392.

Ambrose, S.H., 2002. Small things remembered: origins of early microlithic industries in sub-Saharan Africa. In: Elston, R.G., Kuhn, S.L. (Eds.), Thinking Small: Global Perspectives on Microlithization. Archeological Papers of the American Anthropological Association, vol. 12, pp. 9–30.

Anovitz, L.M., Elam, J.M., Riciputi, L.R., Cole, D.R., 1999. The failure of obsidian hydration dating: sources, implications, and new directions. J. Archaeol. Sci. 26, 735–752.

Arnold, L.J., Roberts, R.G., 2009. Stochastic modelling of multi-grain equivalent dose (D_e) distributions: implications for OSL dating of sediment mixtures. Quatern. Geochronol. 4, 204–230.

Bar-Matthews, M., Marean, C.W., Jacobs, Z., Karkanas, P., Fisher, E.C., Herries, A.I.R., Brown, K., Williams, H.M., Bernatchez, J., Ayalon, A., Nilssen, P.J., 2010. A high resolution and continuous isotopic speleothem record of paleoclimate and paleoenvironment from 90 to 53 ka from pinnacle point on the south coast of South Africa. Quatern. Sci. Rev. 29, 2131–2145.

Bergner, A.G.N., Strecker, M.R., Trauth, M.H., Deino, A., Gasse, F., Blisniuk, P., Dühnforth, M., 2009. Tectonic versus climate influences on the evolution of the lakes in the Central Kenya rift. Quatern. Sci. Rev. 28, 2804–2816.

Bergner, A.G.N., Trauth, M.H., 2004. Comparison of the hydrologic and hydrochemical evolution of Lake Naivasha (Kenya) during three highstands between 175 and 60 kyr BP. Palaeogeogr. Palaeoclimatol. Palaeoecol. 215, 17–36.

Bird, M.I., Turney, C.S.M., Fifield, L.K., Smith, M.A., Miller, G.H., Roberts, R.G., Magee, J.W., 2003. Radiocarbon dating of organic- and carbonate-carbon in *Genyornis* and *Dromaius* eggshell using stepped combustion and stepped acidification. Quatern. Sci. Rev. 22, 1805–1812.

Bøtter-Jensen, L., Andersen, C.E., Duller, G.A.T., Murray, A.S., 2003. Developments in radiation, stimulation and observation facilities in luminescence measurements. Radiat. Meas. 37, 535–541.

Bøtter-Jensen, L., Mejdahl, V., 1988. Assessment of beta dose-rate using a GM multicounter system. Nucl. Tracks Rad. Meas. 14, 187–191.

Bronk Ramsey, C., 2008. Radiocarbon dating: revolutions in understanding. Archaeometry 50, 249–275.

Bronk Ramsey, C., Higham, T., Bowles, A., Hedges, R., 2004. Improvements to the pretreatment of bone at Oxford. Radiocarbon 46, 155–163.

Buylaert, J.P., Murray, A.S., Thomsen, K.J., Jain, M., 2009. Testing the potential of an elevated temperature IRSL signal from K-feldspar. Radiat. Meas. 44, 560–565.

Castañeda, I.S., Werne, J.P., Johnson, T.C., 2007. Wet and arid phases in the southeast African tropics since the Last Glacial maximum. Geology 35, 823–826.

Castañeda, I.S., Werne, J.P., Johnson, T.C., Filley, T.R., 2009. Late Quaternary vegetation history of southeast Africa: the molecular isotopic record from Lake Malawi. Palaeogeogr. Palaeoclimatol. Palaeoecol. 275, 100–112.

Cheng, H., Edwards, R.L., Murrell, M.T., Benjamin, T.M., 1998. Uranium-thorium-protactinium dating systematics. Geochim. Cosmochim. Acta 62, 3437–3452.

Choi, J.H., Duller, G.A.T., Wintle, A.G., Cheong, C.-S., 2006. Luminescence characteristics of quartz from the southern Kenyan Rift Valley: dose estimation using LM-OSL SAR. Radiat. Meas. 41, 847–854.

Clarkson, C., Petraglia, M., Korisettar, R., Haslam, M., Boivin, N., Crowther, A., Ditchfield, P., Fuller, D., Miracle, P., Harris, C., Connell, K., James, H., Koshy, J., 2009. The oldest and longest enduring microlithic sequence in India: 35 000 years of modern human occupation and change at the Jwalapuram locality 9 rockshelter. Antiquity 83, 326–348.

Cohen, A.S., Stone, J.R., Beuning, K.R.M., Park, L.E., Reinthal, P.N., Dettman, D., Scholz, C.A., Johnson, T.C., King, J.W., Talbot, M.R., Brown, E.T., Ivory, S.J., 2007. Ecological consequences of early Late Pleistocene megadroughts in tropical Africa. Proc. Natl. Acad. Sci. 104, 16422–16427.

Conard, N.J., 2005. An overview of the patterns of behavioural change in Africa and Eurasia during the Middle and Late Pleistocene. In: D'Errico, F., Blackwell, L. (Eds.), From Tools to Symbols: From Early Hominids to Modern Humans. Witwatersrand University Press, Johannesburg, pp. 294–332.

David, B., Roberts, R.G., Magee, J., Mialanes, J., Turney, C., Bird, M., White, C., Fifield, K.L., Tibby, J., 2007. Sediment mixing at Nonda Rock: investigations of stratigraphic integrity at an early archaeological site in northern Australia, and implications for the human colonisation of the continent. J. Quatern. Sci. 22, 449–479.

Deacon, H.J., Deacon, J., 1999. Human Beginnings in South Africa: Uncovering the Secrets of the Stone Age. David Philip, Cape Town.

Diez-Martín, F., Domínguez-Rodrigo, M., Sánchez, P., Mabulla, A.Z.P., Tarriño, A., Barba, R., Prendergast, M.E., Luque, L., 2009. The Middle to Later Stone Age technological transition in East Africa: new data from Mumba Rockshelter Bed V (Tanzania) and their implications for the origin of modern human behavior. J. Afr. Archaeol. 7, 147–173.

Eriksson, M.G., Olley, J.M., Payton, R.W., 2000. Soil erosion history in central Tanzania based on OSL dating of colluvial and alluvial hillslope deposits. Geomorphology 36, 107–128.

Fattahi, M., Stokes, S., 2003. Dating volcanic and related sediments by luminescence methods: a review. Earth Sci. Rev. 62, 229–264.

Feathers, J.K., Holliday, V.T., Meltzer, D.J., 2006. Optically stimulated luminescence dating of southern high plains archaeological sites. J. Archaeol. Sci. 33, 1651–1665.

Feathers, J., Kipnis, R., Piló, L., Arroyo-Kalin, M., Coblentz, D., 2010. How old is Luzia? Luminescence dating and stratigraphic integrity at Lapa Vermelha, Lagoa Santa, Brazil. Geoarchaeology 25, 395–436.

Galbraith, R.F., Roberts, R.G., Laslett, G.M., Yoshida, H., Olley, J.M., 1999. Optical dating of single and multiple grains of quartz from Jinmium rock shelter, northern Australia: Part I, experimental design and statistical models. Archaeometry 41, 339–364.

Gliganic, L.A., Jacobs, Z., Roberts, R.G., 2012. Luminescence characteristics and dose distributions for quartz and feldspar grains from Mumba rockshelter, Tanzania. Archaeol. Anthropol. Sci.. doi:10.1007/s12520-011-0085-9.

Grün, R., 2006. Direct dating of human fossils. Yearb. Phys. Anthropol. 49, 2–48.

Grün, R., Aubert, M., Hellstrom, J., Duval, M., 2010. The challenge of direct dating old human fossils. Quatern. Int. 223–224, 87–93.

Hedges, R.E.M., van Klinken, G.J., 1992. A review of current approaches in the pretreatment of bone for radiocarbon dating by AMS. Radiocarbon 34, 279–291.

Henshilwood, C.S., 2008. Winds of change: palaeoenvironments, material culture and human behaviour in the Late Pleistocene (~77 ka–48 ka ago) in the Western Cape Province, South Africa. S. Afr. Archaeol. Soc. Goodwin Ser. 10, 35–51.

Henshilwood, C.S., Marean, C.W., 2003. The origin of modern human behavior: critique of the models and their test implications. Curr. Anthropol. 44, 627–652.

Higham, T.F.G., Jacobi, R.M., Bronk Ramsey, C., 2006. AMS radiocarbon dating of ancient bone using ultrafiltration. Radiocarbon 48, 179–195.

Huntley, D.J., Baril, M.R., 1997. The K content of the K-feldspars being measured in optical dating or in thermoluminescence dating. Ancient TL 15, 11–13.

Huntley, D.J., Godfrey-Smith, D.I., Thewalt, M.L.W., 1985. Optical dating of sediments. Nature 313, 105–107.

Huntley, D.J., Hancock, R.G.V., 2001. The Rb contents of the K-feldspar grains being measured in optical dating. Ancient TL 19, 43–46.

Huntley, D.J., Lamothe, M., 2001. Ubiquity of anomalous fading in K-feldspars and the measurement and correction for it in optical dating. Can. J. Earth Sci. 38, 1093–1106.

Jacobs, Z., Duller, G.A.T., Wintle, A.G., 2006a. Interpretation of single grain D_e distributions and calculation of D_e. Radiat. Meas. 41, 264–277.

Jacobs, Z., Duller, G.A.T., Wintle, A.G., Henshilwood, C.S., 2006b. Extending the chronology of deposits at Blombos Cave, South Africa, back to 140 ka using optical dating of single and multiple grains of quartz. J. Hum. Evol. 51, 255–273.

Jacobs, Z., Meyer, M.C., Roberts, R.G., Aldeais, V., Dibble, H., El Hajraoui, M.A., 2011. Single-grain OSL dating at La Grotte des Contrebandiers ('Smugglers Cave'), Morocco: improved age constraints for the Middle Paleolithic levels. J. Archaeol. Sci. 38, 3631–3643.

Jacobs, Z., Roberts, R.G., 2007. Advances in optically stimulated luminescence dating of individual grains of quartz from archeological deposits. Evol. Anthropol. 16, 210–223.

Jacobs, Z., Roberts, R.G., 2009. Human history written in stone and blood. Am. Sci. 97, 302–309.

Jacobs, Z., Roberts, R.G., Galbraith, R.F., Deacon, H.J., Grün, R., Mackay, A., Mitchell, P., Vogelsang, R., Wadley, L., 2008a. Ages for the Middle Stone Age of southern Africa: implications for human behavior and dispersal. Science 322, 733–735.

Jacobs, Z., Wintle, A.G., Duller, G.A.T., 2006c. Evaluation of SAR procedures for D_e determination using single aliquots from two archaeological sites in South Africa. Radiat. Meas. 41, 520–533.

Jacobs, Z., Wintle, A.G., Roberts, R.G., Duller, G.A.T., 2008b. New ages for the post-Howiesons Poort, late and final Middle Stone Age at Sibudu, South Africa. J. Archaeol. Sci. 35, 1790–1807.

Jacobs, Z., Wintle, A.G., Roberts, R.G., Duller, G.A.T., 2008c. Equivalent dose distributions from single grains of quartz at Sibudu, South Africa: context, causes and consequences for optical dating of archaeological deposits. J. Archaeol. Sci. 35, 1808–1820.

Köhl-Larsen, L., 1943. Auf den Spuren des Vormenschen. Strecker und Schröeder Verlag, Stuttgart.

Mabulla, A.Z.P., 2007. Hunting and foraging in the Eyasi basin, northern Tanzania: past, present and future prospects. Afr. Archaeol. Rev. 24, 15–33.

Mackay, A., 2011. Nature and significance of the Howiesons Poort to post-Howiesons Poort transition at Klein Kliphuis rockshelter, South Africa. J. Archaeol. Sci. 38, 1430–1440.

Manega, P.C., 1993. Geochronology, Geochemistry, and Isotopic Study of the Plio-Pleistocene Hominid Sites and the Ngorongoro Volcanic Highland in Northern Tanzania. Ph.D. Dissertation, University of Colorado.

McBrearty, S., Brooks, A.S., 2000. The revolution that wasn't: a new interpretation of the origin of modern human behavior. J. Hum. Evol. 39, 453–563.
McCall, G.S., 2007. Behavioral ecological models of lithic technological change during the later Middle Stone Age of South Africa. J. Archaeol. Sci. 34, 1738–1751.
Mehlman, M.J., 1989. Late Quaternary Archaeological Sequences in Northern Tanzania. Ph.D. Dissertation, University of Illinois.
Mejdahl, V., 1979. Thermoluminescence dating: beta-dose attenuation in quartz grains. Archaeometry 21, 61–72.
Mellars, P., 2006. Why did modern human populations disperse from Africa ca. 60,000 years ago? A new model. Proc. Natl. Acad. Sci. 103, 9381–9386.
Mercier, N., Falguéres, C., 2007. Field gamma dose-rate measurement with a NaI(Tl) detector: re-evaluation of the 'threshold' technique. Ancient TL 25, 1–4.
Murray, A.S., Wintle, A.G., 2000. Luminescence dating of quartz using an improved single-aliquot regenerative-dose protocol. Radiat. Meas. 32, 57–73.
Murray, A.S., Wintle, A.G., 2003. The single-aliquot regenerative-dose protocol: potential for improvements in reliability. Radiat. Meas. 37, 377–381.
Olley, J.M., Murray, A.S., Roberts, R.G., 1996. The effects of disequilibria in the uranium and thorium decay chains on burial dose rates in fluvial sediments. Quatern. Sci. Rev. 15, 751–760.
Olley, J.M., Roberts, R.G., Murray, A.S., 1997. Disequilibria in the uranium decay series in sedimentary deposits at Allen's Cave, Nullarbor Plain, Australia: implications for dose rate determinations. Radiat. Meas. 27, 433–443.
Olley, J.M., Roberts, R.G., Yoshida, H., Bowler, J.M., 2006. Single-grain optical dating of grave-infill associated with human burials at Lake Mungo, Australia. Quatern. Sci. Rev. 25, 2469–2474.
Petraglia, M., Clarkson, C., Boivin, N., Haslam, M., Korisettar, R., Chaubey, G., Ditchfield, P., Fuller, D., James, H., Jones, S., Kivisild, T., Koshy, J., Lahr, M.M., Metspalu, M., Roberts, R., Arnold, L., 2009. Population increase and environmental deterioration correspond with microlithic innovations in South Asia ca. 35,000 years ago. Proc. Natl. Acad. Sci. 106, 12261–12266.
Pike, A.W.G., Hedges, R.E.M., van Calsteren, P., 2002. U-series dating of bone using the diffusion-absorption model. Geochim. Cosmochim. Ac 66, 4273–4286.
Prendergast, M.E., Luque, L., Domínguez-Rodrigo, M., Diez-Martín, F., Mabulla, A.Z.P., Barba, R., 2007. New excavations at Mumba rockshelter, Tanzania. J. Afr. Archaeol. 5, 217–243.
Prescott, J.R., Hutton, J.T., 1994. Cosmic ray contributions to dose rates for luminescence and ESR dating: large depths and long-term time variations. Radiat. Meas. 23, 497–500.
Readhead, M.L., 1987. Thermoluminescence dose rate data and dating equations for the case of disequilibrium in the decay series. Nucl. Tracks Radiat. Meas. 13, 197–207.
Reimer, P.J., Baillie, M.G.L., Bard, E., Bayliss, A., Beck, J.W., Bertrand, C.J.H., Blackwell, P.G., Buck, C.E., Burr, G.S., Cutler, K.B., Damon, P.E., Edwards, R.L., Fairbanks, R.G., Friedrich, M., Guilderson, T.P., Hogg, A.G., Hughen, K.A., Kromer, B., McCormac, G., Manning, S., Ramsey, C.B., Reimer, R.W., Remmele, S., Southon, J.R., Stuiver, M., Talamo, S., Taylor, F.W., van der Plicht, J., Weyhenmeyer, C.E., 2004. IntCal04 terrestrial radiocarbon age calibration, 0–26 cal kyr BP. Radiocarbon 46, 1029–1058.
Reimer, P.J., Baillie, M.G.L., Bard, E., Bayliss, A., Beck, J.W., Blackwell, P.G., Bronk Ramsey, C., Buck, C.E., Burr, G.S., Edwards, R.L., Friedrich, M., Grootes, P.M., Guilderson, T.P., Hajdas, I., Heaton, T.J., Hogg, A.G., Hughen, K.A., Kaiser, K.F., Kromer, B., McCormac, F.G., Manning, S.W., Reimer, R.W., Richards, D.A., Southon, J.R., Talamo, S., Turney, C.S.M., van der Plicht, J., Weyhenmeyer, C.E., 2009. IntCal09 and Marine09 radiocarbon age calibration curves, 0–50,000 years cal BP. Radiocarbon 51, 1111–1150.
Rhodes, E.J., Schwenninger, J.-L., 2007. Dose rates and radioisotope concentrations in the concrete calibration blocks at Oxford. Ancient TL 25, 5–8.
Richardson, J.L., Dussinger, R.A., 1986. Paleolimnology of mid-elevation lakes in the Kenya Rift Valley. Hydrobiologia 143, 167–174.
Ridings, R., 1996. Where in the world does obsidian hydration dating work? Am. Antiq. 61, 136–148.
Roberts, R., Bird, M., Olley, J., Galbraith, R., Lawson, E., Laslett, G., Yoshida, H., Jones, R., Fullagar, R., Jacobsen, G., Hua, Q., 1998. Optical and radiocarbon dating at Jinmium rock shelter in northern Australia. Nature 393, 358–362.
Roberts, R.G., Galbraith, R.F., Olley, J.M., Yoshida, H., Laslett, G.M., 1999. Optical dating of single and multiple grains of quartz from Jinmium rock shelter, northern Australia: Part II, results and implications. Archaeometry 41, 365–395.
Roberts, R.G., Galbraith, R.F., Yoshida, H., Laslett, G.M., Olley, J.M., 2000. Distinguishing dose populations in sediment mixtures: a test of single-grain optical dating procedures using mixtures of laboratory-dosed quartz. Radiat. Meas. 32, 459–465.
Scholz, C.A., Cohen, A.S., Johnson, T.C., King, J., Talbot, M.R., Brown, E.T., 2011. Scientific drilling in the Great Rift Valley: the 2005 Lake Malawi Scientific Drilling Project – an overview of the past 145,000 years of climate variability in Southern Hemisphere East Africa. Palaeogeogr. Palaeoclimatol. Palaeoecol. 303, 3–19.
Scholz, C.A., Johnson, T.C., Cohen, A.S., King, J.W., Peck, J.A., Overpeck, J.T., Talbot, M.R., Brown, E.T., Kalindekafe, L., Amoako, P.Y.O., Lyons, R.P., Shanahan, T.M., Castañeda, I.S., Heil, C.W., Forman, S.L., McHargue, L.R., Beuning, K.R., Gomez, J., Pierson, J., 2007. East African megadroughts between 135 and 75 thousand years ago and bearing on early-modern human origins. Proc. Natl. Acad. Sci. 104, 16416–16421.
Skinner, A.R., Hay, R.L., Masao, F., Blackwell, B.A.B., 2003. Dating the Naisiusiu Beds, Olduvai Gorge, by electron spin resonance. Quatern. Sci. Rev. 22, 1361–1366.
Smith, M.A., Prescott, J.R., Head, M.J., 1997. Comparison of ^{14}C and luminescence chronologies at the Puritjarra rock shelter, central Australia. Quatern. Sci. Rev. 16, 299–320.
Stafford Jr., T.W., Hare, P.E., Currie, L., Jull, A.J.T., Donahue, D.J., 1991. Accelerator radiocarbon dating at the molecular level. J. Archaeol. Sci. 18, 35–72.
Surovell, T.A., 2000. Radiocarbon dating of bone apatite by step heating. Geoarchaeology 15, 591–608.
Taylor, R.E., 1987. Radiocarbon Dating: An Archaeological Perspective. Academic Press, Orlando.
Thomsen, K.J., Murray, A.S., Jain, M., Bøtter-Jensen, L., 2008. Laboratory fading rates of various luminescence signals from feldspar-rich sediment extracts. Radiat. Meas. 43, 1474–1486.
Tierney, J.E., Russell, J.M., Damsté, J.S.S., Huang, Y., Verschuren, D., 2011. Late Quaternary behaviour of the East African monsoon and the importance of the Congo Air Boundary. Quatern. Sci. Rev. 30, 798–807.
Tierney, J.E., Russell, J.M., Huang, Y., 2010. A molecular perspective on Late Quaternary climate and vegetation change in the Lake Tanganyika basin, East Africa. Quatern. Sci. Rev. 29, 787–800.
Tierney, J.E., Russell, J.M., Huang, Y., Damsté, J.S.S., Hopmans, E.C., Cohen, A.S., 2008. Northern Hemisphere controls on tropical southeast African climate during the past 60,000 years. Science 322, 252–255.
Trauth, M.H., Deino, A.L., Bergner, A.G.N., Strecker, M.R., 2003. East African climate change and orbital forcing during the last 175 kyr BP. Earth Planet. Sci. Lett. 206, 297–313.
Tsukamoto, S., Rink, W.J., Watanuki, T., 2003. OSL of tephric loess and volcanic quartz in Japan and an alternative procedure for estimating D_e from a fast OSL component. Radiat. Meas. 37, 459–465.
Westaway, K.E., Roberts, R.G., 2006. A dual-aliquot regenerative-dose protocol (DAP) for thermoluminescence (TL) dating of quartz sediments using the light-sensitive and isothermally stimulated red emissions. Quatern. Sci. Rev. 25, 2513–2528.
Wintle, A.G., 1973. Anomalous fading of thermoluminescence in mineral samples. Nature 245, 143–144.
Wintle, A.G., 1997. Luminescence dating: laboratory procedures and protocols. Radiat. Meas. 27, 769–817.
Wright, D.K., Forman, S.L., Kusimba, C.M., Pierson, J., Gomez, J., Tattersfield, P., 2007. Stratigraphic and geochronological context of human habitation along the Galana River, Kenya. Geoarchaeology 22, 708–728.
Wurz, S., 1999. The Howiesons Poort backed artifacts from Klasies River: an argument for symbolic behavior. S. Afr. Archaeol. Bull. 54, 38–50.